Chemical Geology 285 (2011) 231–255

Contents lists available at ScienceDirect

Chemical Geology

journal homepage: www.elsevier.com/locate/chemgeo

Provenance and paleoweathering reconstruction of the Neoproterozoic Johnnie Formation, southeastern California

William A. Schoenborn [a,*], Christopher M. Fedo [b]

[a] Department of Earth and Environmental Science, The George Washington University, Washington, DC, 20052 USA
[b] Department of Earth and Planetary Sciences, University of Tennessee, Knoxville TN 37996, USA

ARTICLE INFO

Article history:
Received 29 November 2010
Received in revised form 18 April 2011
Accepted 19 April 2011
Available online 27 April 2011

Editor: U. Brand

Keywords:
Neoproterozoic
Johnnie Formation
Provenance
Paleoweathering

ABSTRACT

Petrologic and geochemical data confirm that mudstones and sandstones of the Johnnie Formation were the initial siliciclastic deposits laid along the Cordilleran Laurentian margin following the Neoproterozoic break-up of Rodinia. Sedimentary rocks of the Johnnie Formation have corrected CIA values between 63 and 83 (or higher), which suggest moderate to intense weathering of crystalline source rocks or recycling. Based on modeling the fresh source rocks likely consisted of 90% granodiorite and 10% high-K granite. This conclusion is based on petrographic observations, major element geochemistry, and investigation of the REE: ($La_{CN}/Sm_{CN} = 4.19 \pm 1.26$, $Gd_{CN}/Yb_{CN} = 1.34 \pm 0.38$, $Eu/Eu^* = 0.63 \pm 0.09$ and $La_{CN}/Yb_{CN} = 9.55 \pm 2.27$). Feldspars are unevenly distributed in the finer grained sedimentary rocks. Observed fluctuations in feldspar content throughout the Johnnie Formation are interpreted as a result of abrasion and hydrodynamic sorting, which concentrated feldspars in the finer grained sediment. None of the mudstone samples, including those collected just below and above the flat-pebble conglomerate in the upper Johnnie Formation, show evidence of true cold weather depositional conditions. Consequently, Johnnie Formation mudstone geochemistry does not record evidence of an extreme paleoclimatic environmental shift in the succession. Textural characteristics of Johnnie Formation sandstones are consistent with quiescent tectonic conditions characterized by low relief, and deposition of Johnnie Formation strata in a passive-margin setting.

Published by Elsevier B.V.

1. Introduction

The composition of clastic sedimentary rocks results from the combined effects of many factors active during sediment production, including source rock composition, physical and chemical weathering, transport, deposition and diagenesis (Johnsson, 1993). Chemical weathering progressively modifies the mineralogical composition of crystalline bedrock by turning primary minerals into clays, secondary oxides, and hydroxides (Nesbitt and Young, 1984, 1989). These secondary minerals, in addition to quartz, represent the mineral assemblage developed atop fresh bedrock that is subject to mass wasting, transport, and hydraulic sorting. Therefore, the mineralogical maturity of sediment largely reflects the composition of weathering profiles (Nesbitt et al., 1996, 1997), where the degree of conversion of feldspars to secondary aluminous clays is related to paleoweathering intensity, paleoclimate (cf., Fedo et al., 1996, 1997b; Nesbitt et al., 1997), and tectonism (e.g., Hurowitz and McLennan, 2005).

In western North America, the Neoproterozoic-to-Cambrian continental margin succession preserves evidence related to both paleoclimate and tectonic setting. Several significant events are encompassed by these strata including breakup of the supercontinent Rodinia (Dalziel, 1991, 1997; Moores, 1991; Borg and DePaolo, 1994; Buchan et al., 2001; Karlstrom et al., 2001; Eyles and Januszczak, 2004; Li et al., 2008), and at least two episodes of widespread glaciation that may have extended to equatorial regions (Young, 1995; Hoffman et al., 1998; Williams, et al., 1998; Crowell, 1999; Prave, 1999; Sohl, et al., 1999, Hoffman and Schrag, 2002), including cap carbonates (Kaufman et al., 1992, 1993, 1997; Corsetti and Kaufman, 2003). The distribution and lithologic characteristics of Neoproterozoic and Cambrian age strata suggest that the crust was initially thinned, underwent a complex rifting process (Ferri et al., 1999; Prave, 1999), then was covered by a thick sedimentary sequence typical of stable continental margins (Stewart, 1972; Link et al., 1993; Fedo and Cooper, 2001). This succession includes glaciogenic diamictites of the Kingston Peak Formation (Wright et al., 1976; Miller, 1985, 1986; Prave, 1999) overlain by siliciclastic and subordinate carbonate rocks. Evidence for rifting exists in Kingston Peak diamictites (Wright et al., 1976; Miller, 1985, 1986; Walker et al., 1986), and possibly extends into the post-glaciogenic detrital sequence immediately above (Bond et al., 1985; Link et al., 1993; Summa, 1993; Clapham and Corsetti, 2005). The post-glaciogenic sequence is comprised predominantly of siliciclastic deposits, initiated by the Johnnie Formation, that were deposited above storm wave base in shallow marine and terrestrial settings (Levy and Christie-Blick, 1991; Summa, 1993; Fedo and

* Corresponding author at: U.S. Environmental Protection Agency, Washington, DC, 20460, USA.
E-mail address: schoenborn.william@epa.gov (W.A. Schoenborn).

0009-2541/$ – see front matter. Published by Elsevier B.V.
doi:10.1016/j.chemgeo.2011.04.014

Cooper, 2001). Quartz-to-feldspar ratios in arenites comprising the post-Kingston Peak succession change repeatedly (Link et al., 1993), questioning whether compositional variation can be solely attributed to tectonic causes. Variable feldspar content in post-Kingston Peak arenites could also have been influenced by fluctuating climatic conditions because, by Cambrian time, the region had migrated from high to low latitudes (McKerrow et al., 1992; Dalziel, 1997; Weil et al., 1998; Hodych et al., 2004; Cawood and Pisarevsky, 2006; Li et al., 2008).

Post-glacial cap carbonates with significant negative $\delta^{13}C$ anomalies that possibly record extreme shifts in paleoclimate occur in the Noonday Dolomite, which rests atop Kingston Peak diamictite, as well as in carbonates within the younger post-glaciogenic siliciclastic succession. The largest excursion ($\delta^{13}C = -11‰$ PDB) is preserved in carbonates interbedded with detrital rocks of the Rainstorm Member of the upper Johnnie Formation, located well above the Kingston Peak Formation, and not associated with any glacial unit (Corsetti and Kaufman, 2003). Associated with these carbonates are incised

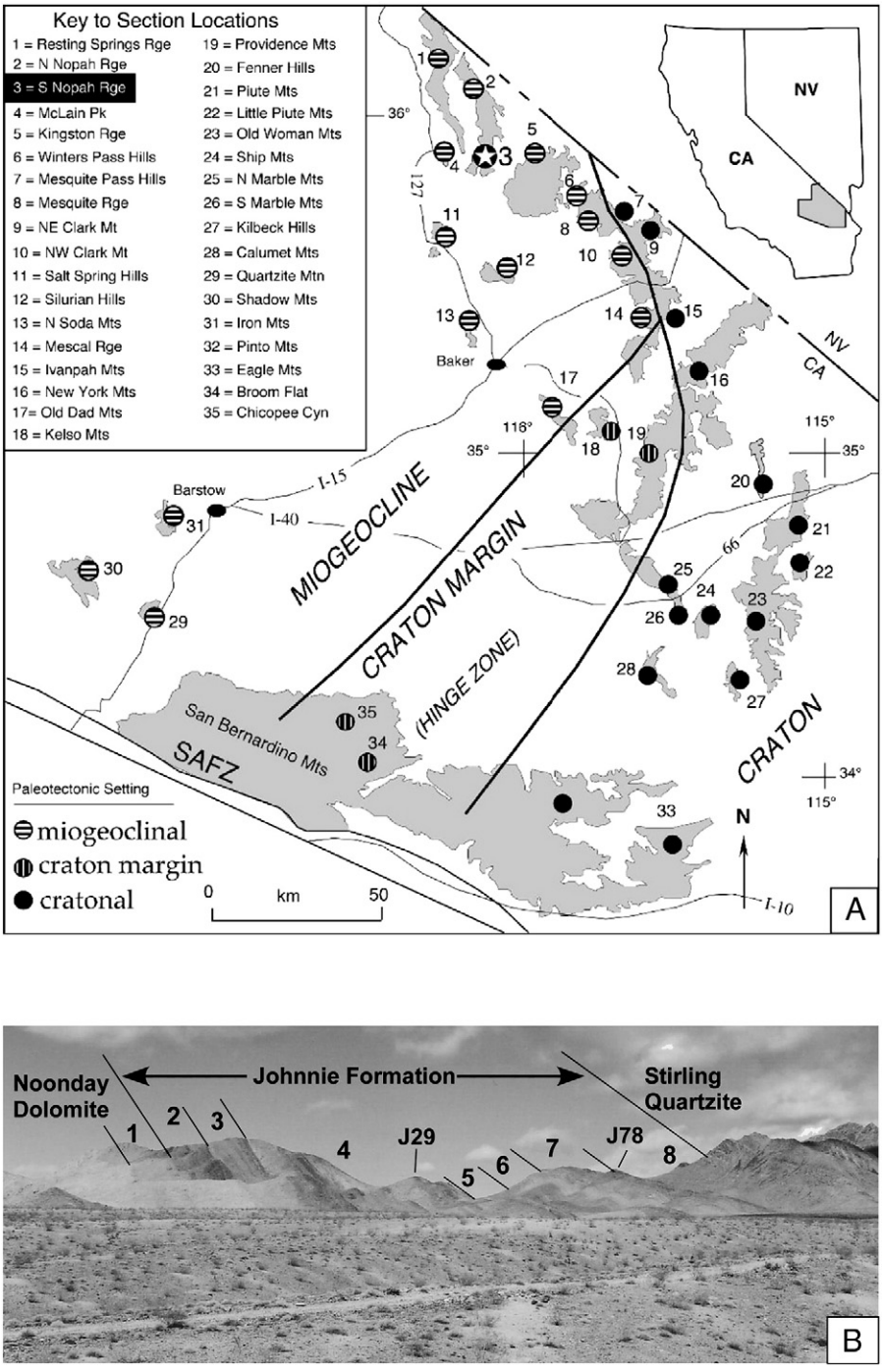

Fig. 1. (A) Index map showing location of study area in the Nopah Range (Station 3, black highlight) relative to the Precambrian cratonic margin in southeastern California (after Fedo and Cooper, 2001). (B) Photograph of stratigraphic section looking northwest along the Noonday mine road (location: N35° 48.861′, W116° 06.243′) showing major stratigraphic units (Noonday Dolomite, Johnnie Formation, and Stirling Quartzite) along with subunits of the Johnnie Formation. Sample J78 is located at the base of the incised valley fill (flat-pebble conglomerate).

valleys with significant relief (> 75 m; Summa, 1993) of probable glacial origin (Abolins et al., 2000), although a tectonic driver has also been suggested (Clapham and Corsetti, 2005).

In this paper, we examine dominantly siliciclastic strata of the Late Neoproterozoic Johnnie Formation in the Death Valley region (Fig. 1A) in an effort to: 1) determine the composition of mudstones and sandstones of the Johnnie Formation; 2) evaluate diagenetic changes to sediment composition after burial; and 3) deduce the provenance and paleoweathering conditions that affected sediments comprising the Johnnie Formation in order to help decipher the evolution of the Laurentian margin. The results of this study contribute to our understanding of prevailing paleoclimatic conditions during deposition of the Johnnie Formation and provide data relevant to the formation of Laurentia.

2. Stratigraphic setting

Stewart (1970) recognized the Johnnie Formation as a regional stratigraphic unit covering ~26,000 km^2 that thickens in a westward direction from approximately 200 m to 1500 m. Strata of the Johnnie Formation comprise a heterogeneous succession of laterally variable siltstone, quartzite, conglomerate, sandstone, and dolomite representing both marine and non-marine depositional environments. Summa (1993) and Fedo and Cooper (2001) described the Johnnie Formation as a mixed siliciclastic-carbonate succession deposited under fluvially influenced shallow-marine conditions. The continental margin was dominated by a low-gradient braided-fluvial system that debouched siliciclastic sediment into a low-energy inner-shelf basin, bounded by carbonate source areas that supplied allochems to the basin where carbonate and siliciclastic material mixed (Summa, 1993).

For this geochemical investigation, the Johnnie Formation is subdivided into seven subunits, designated Units 2 through 8, based on distinct facies (Fig. 1B). In the sampled section, the entire Rainstorm Member, including the Johnnie oolite, has been removed by erosion and replaced by a coarse flat-pebble conglomerate interpreted as an incised valley fill (Summa, 1993; sample J78, Fig. 1B).

3. Sampling and analytical techniques

Sixty-two samples of fresh sandstone and mudstone were collected for analysis from a measured stratigraphic section (nearly 100% exposed) of the Johnnie Formation (Fig. 2) in the southern Nopah Range, California. Samples were collected in pairs where possible, one sandstone and one mudstone, in order to aid in assessing similarities and differences related to grain size. Twenty-six polished thin sections were made of representative sandstone and mudstone for petrographic and electron microprobe analysis. Powders were prepared in a shatterbox using a ceramic dish/puck and analyzed at the Advanced Centre for Queensland University Isotope Research Excellence (AQUIRE) in Queensland, Australia for major- and trace-element analyses on a PE3300 DV ICP-OES and Fisons PQ2 + ICP-MS. For each analysis, instrument responses were calibrated against that of JGS reference materials JR2, JG2, JA-3 and JB3. For all major oxides but SiO_2, the average estimated errors on the totals are less than 1%; for SiO_2 the error is <1%–3% with 2% being the error in Si itself. Internal errors on all elements were better than 1% except for Tl, Cd, Sn, and Sb. Reference standard JA-3 was run as an unknown to estimate data reproducibility. The long term average of JA-3 yields ~1% to 1.5% reproducibility for all elements. Analytical results are displayed in Table 1.

Quantitative electron microprobe analyses of major and minor elements in feldspars were obtained at U.S. Geological Survey, Reston, VA with a JEOL JXA-8900 five spectrometer, fully automated electron probe microanalyzer using wavelength-dispersive X-ray spectrometry. Analyses were made at 15 keV accelerating voltage and 20 nA probe current measured with a Faraday cup; counting times on both peak and background varied from 20 to 120 s, with a 5 μm diameter probe spot. Analyses were corrected for electron beam matrix effects, instrumental drift, and deadtime using a ZAF algorithm as supplied with the JEOL JXA-8900 electron microprobe. Relative accuracy of the analyses, based upon comparison between measured and published compositions of standard USGS reference materials, is ~1–2% for oxide concentration >1 wt.% and ~5–10% for oxide concentrations <1 wt.%. Elements analyzed as oxides and their detection limits (wt.%) at 3σ range from 0.04 to 0.01 wt.%. Analytical results from representative samples are displayed in Table 2.

4. Petrography

4.1. Composition

Arenites of the Johnnie Formation are comprised of variable amounts of feldspar, <5% lithic fragments, and monocrystalline quartz (Figs. 3, 4; Table 3). Accessory minerals include zircon, tourmaline, rutile, apatite, and muscovite. Modal proportions of plagioclase and K-feldspar increase upsection (Fig. 3) and vary from fresh-to-weathered. Lithic fragments occur as durable grains of chert or metaquartzite (Fig. 4B, C). Ratios of monocrystalline quartz to feldspar (Q_m/F) decrease from 237 in one Unit 2 arenite to ~1 in arenites of Units 6 and 7 (Fig. 3), whereas median quartz grain size generally decreases upsection from coarse to fine sand. In strata of Units 2 to 4, feldspars are chiefly isolated grains of subhedral orthoclase and microcline that comprise less than 1% of grains present; they are partly to wholly replaced by white mica. In arenites of Unit 5, rounded feldspar grains comprise 3% to 24% of the rocks and are composed exclusively of albite. Feldspars in arenites of Units 6 and 7 include both plagioclase and K-feldspar similar in grain size to associated quartz, and comprise >20% of modal mineralogy (Fig. 4D). Plagioclase-to-K-feldspar ratios in lower Johnnie Formation sediment are low (P/K = 0–0.2), but generally increase in middle and upper parts of the formation (Units exclusive of Unit 5: P/K = 0.3–1.9). Just below the base of Unit 8, sandstone samples are distinctly arkosic with plagioclase and K-feldspar each comprising ~20% of the terrigenous mineral content (Fig. 3).

Feldspar compositions were determined by electron microprobe for 292 grains representing the whole section (539 analyses total, averaging 15 grains per slide, including analysis of core and rim for most grains; Table 2; see Schoenborn (2010) for all analyses). K-feldspar compositions are relatively pure (>Or_{90}), whereas most plagioclase compositions range from oligoclase (Ab_{73}) to nearly pure albite (>Ab_{99}) (Fig. 5). Most grains exhibit no compositional differences between core and rim. Grains with nearly pure end member compositions typical of authigenic albite (>Ab_{98}) constitute a common (22% of grains) subpopulation.

4.2. Textures

Johnnie Formation sandstone is classed as poorly sorted, medium to slightly pebbly, texturally submature quartzarenite to arkose (Fig. 6A). Fabrics are commonly homogenous and tightly packed. Quartz grains are, on average, subangular, but vary from angular to well rounded. Many large grains exhibit well rounded cores with secondary quartz cement overgrowths (Fig. 4A). Throughout the studied section, feldspar grains, which are concentrated in the fine sandstone (Fig. 6A, B), are mostly angular, but some are subrounded to rounded.

In the lower Johnnie Formation there is no variation in roundness as all samples contain the same mixed assemblage of rounded to angular quartz. In contrast, some quartzites of the middle Johnnie Formation (Unit 4: J36A and J39A) are composed mostly of rounded to well rounded coarse sand grains, and display evidence of rounding of

Column Sample Number	Lithologic Description	Depositional Environment (Summa, 1993)
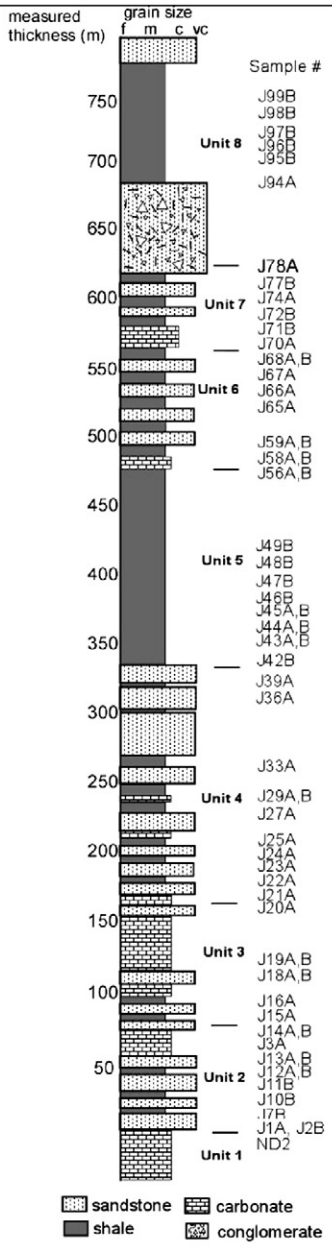	Unit 8: Coarse flat pebble conglomerate overlain by predominantly pale bwn to grn-grey shale; interlayered with discontinuous bds of sst. Significant unconformity at base.	Valley-fill breccia and conglomerate overlain by deeper water shale facies.
	Unit 7: Mixed carbonate-siliciclastic unit; ; interlayered with flaggy ppl-red to grn. micaceous siltst. Proportion of carbonate decreases towards top of unit.	Thick intertidal to supratidal microbial laminites grading upward into fluvially influenced shallow marine shelf.
	Unit 6: Mixed sst-siltst unit; alternating continuous tabular thn to med bdd sst, planar laminated, to x-bdd, and flaggy tabular silst, mnr thn sandy carbonate bds	Distal low-energy shallow marine shelf shoaling upward into intertidal to supratidal microbial laminites.
	Unit 5: Thin bdd., flaggy, dk reddish-bwn silty shale-shaly siltst. interlayered with grey siltst.-silty sst.; Shaly layers predominate	Distal open marine shelf generally below fair weather wave base; Upward shoaling.
	Unit 4: Cross-stratified sandstone, med. thick to massive beds; pale yel. grey pinkish grey; interlayered w/ minor dk brown flaggy siltsts. Few sandy carbonate beds	Fluvial braid-plain grading upward to tide-dominated shallow marine facies.
	Unit 3: Carbonate dominated, mixed siliciclastic carbonate unit. sst. med.-thin bdd., planar laminated, tabular, laterally continuous. Interlayered w/ pale olive microbially laminated dolostones.	Fluvially influenced shallow marine shelf outboard of siliciclastic dominated mixed facies.
	Unit 2: (Johnnie Formation-Noonday Dolomite contact and above); Sandstone dominated siliciclastic carbonate unit; Laterally continuous, Med-bdd, planar stratified coarse sst.; interlayered with sltst, poorly sorted sst., and cross-bedded sandy dolostone.; Dolostone. content increases up section. Unit 1: Johnnie Formation-Noonday Dolomite transition (that is, the unit below the Johnnie-ND contact): Mixed thin bdd silty dolostone-carbonate sand; laterally continuous. bds.	Fluvially dominated shallow marine shelf.

Fig. 2. Schematic stratigraphic section of Johnnie Formation with lithologic descriptions and interpreted paleoenvironments. Numbers represent samples collected.

medium to fine-grained quartz sand, perhaps suggesting that some roundness was accomplished at the site of deposition (Folk, 1974).

On the basis of petrographic and geochemical characteristics, sand-size material in the Johnnie Formation may comprise both first- and multi-cycle grains. Arkoses from the middle-to-upper portions of the Johnnie Formation (Units 6 and 7) are fine grained, and preserve fresh feldspar ($Q_m/F \leq 10$). These rocks are similar to first-cycle sands of the Orinoco River basin that are comprised of fine grained angular to subangular quartz, fresh feldspar, and lithic fragments (Johnsson et al., 1988, 1991). In contrast, demonstrably multi-cycle sands delivered by rivers along the Gulf Coast, southern USA, have almost no feldspar, and are comprised of quartz grains that display a high degree of roundness largely inherited from older, poorly consolidated sandstone (Mehring and McBride, 2007). The well rounded quartz grains in lower and middle Johnnie Formation (Units 2 and 4) may have been cannibalized from older sedimentary rocks, so that some of the sand has probably been through more than one sedimentary cycle.

Variations in Zr content (Fig. 7; McLennan et al., 1993) may also indicate that some sandstones of the Johnnie Formation represent first-cycle deposits whereas others have a multi-cycle origin. Some sandstone from Units 6 and 7 have Zr/Sc ratios < 100, suggesting these samples experienced limited amounts of sedimentary sorting and recycling; whereas others have Zr/Sc ratios similar to weathered soil (i.e., first cycle material) from the Toorongo profile, which is developed on granodiorite. The mineralogy and weathering characteristics of the Toorongo profile are analogous to large scale weathering of the

Table 1
Major and trace element analyses of sandstones and mudstones.

	Noonday Dolomite	Johnnie Fm. sandstones								
Sample	ND2R	J1AR	J3AR	J5AR	J9R	J12AR	J13AR	J14A	J15AR	J16AR
Unit	1	2	2	2	2	2	2	2	2	2
SiO_2	7.61	91.49	93.11	80.77	81.43	95.02	90.18	88.32	59.10	82.24
TiO_2	0.06	0.71	0.63	0.58	0.99	0.73	0.50	1.54	0.23	0.26
Al_2O_3	0.67	2.24	0.47	1.30	1.18	1.74	3.58	4.20	0.88	0.36
FeO(t)	0.55	1.04	1.67	1.10	1.74	0.94	1.98	1.59	0.66	0.81
Fe_2O_3	0.62	1.16	1.85	1.22	1.94	1.05	2.20	1.76	0.73	0.90
MnO	0.04	0.02	0.04	0.02	0.07	0.03	0.01	0.01	0.09	0.04
MgO	17.67	0.13	0.12	2.93	2.60	0.17	0.27	0.40	8.61	3.20
CaO	29.22	0.00	0.00	4.05	3.74	0.00	0.22	0.27	12.56	4.48
Na_2O	0.09	0.08	0.12	0.08	0.11	0.11	0.03	0.04	0.12	0.13
K_2O	0.20	0.70	0.18	0.45	0.36	0.58	1.12	1.40	0.25	0.17
P_2O_5	0.05	0.04	0.04	0.05	0.05	0.04	0.07	0.07	0.04	0.03
LOI	44.09	0.76	3.38	6.65	6.11	0.62	1.05	0.90	19.49	7.26
Total	100.87	98.37	101.60	99.21	100.31	101.03	101.21	100.50	102.76	99.90
Li	1.85	4.45	1.86	2.48	3.54	4.51	3.63	6.12	3.15	1.56
Be	0.22	0.23	0.08	0.25	0.19	0.24	0.21	0.44	0.15	0.06
Sc	0.93	1.08	0.94	2.31	1.39	1.38	1.64	2.61	2.34	1.55
Ti	328.71	3575.29	3462.45	3259.67	5484.84	4345.86	2606.58	6806.86	1250.16	1444.31
V	8.21	14.33	14.49	23.52	19.38	22.15	21.80	81.21	16.43	9.06
Cr	3.83	7.00	4.04	6.81	6.12	8.52	7.80	15.43	3.55	2.20
Co	1.31	6.04	2.87	4.02	4.63	8.69	2.83	4.70	1.38	2.76
Ni	4.05	7.39	2.23	6.36	6.90	12.25	2.57	7.48	2.80	3.71
Cu	5.24	30.54	6.19	8.37	9.39	6.51	18.45	35.93	7.81	7.82
Zn	6.94	2.01	3.09	16.46	1.95	1.99	3.84	5.54	16.39	33.76
Ga	1.01	1.81	0.57	2.01	1.59	2.53	2.78	4.33	1.09	0.48
As	0.99	5.05	11.84	12.95	12.42	3.29	9.67	11.21	5.88	6.35
Rb	6.82	14.63	4.02	11.73	10.51	16.03	22.07	28.14	8.34	2.96
Sr	74.96	7.21	4.62	13.29	49.84	9.27	20.95	8.38	76.43	11.09
Y	5.70	7.25	4.02	5.44	5.61	7.86	7.66	7.78	5.20	3.34
Zr	17.43	110.89	78.78	176.66	152.90	141.14	128.67	227.97	125.90	62.47
Nb	0.80	3.38	2.72	3.25	4.69	4.38	2.91	5.93	1.90	1.36
Mo	0.34	0.50	1.44	1.80	2.89	0.34	1.58	3.86	0.59	0.64
Cd	0.02	0.05	0.04	0.11	0.10	0.07	0.06	0.09	0.11	0.29
Sn	0.15	0.31	0.15	0.31	0.25	0.32	0.46	1.49	0.19	0.10
Sb	0.17	0.33	0.70	0.68	0.32	0.18	0.43	2.29	3.53	0.52
Cs	0.22	0.62	0.16	0.35	0.35	0.67	0.55	0.86	0.24	0.12
Ba	25.91	42.69	16.76	27.68	40.67	35.09	57.14	77.36	23.15	8.35
La	4.35	4.55	3.16	8.53	4.20	4.26	11.36	11.51	7.07	2.45
Ce	7.42	9.74	6.98	18.18	9.18	8.54	29.86	28.30	15.88	5.52
Pr	0.99	1.15	0.77	2.09	1.04	0.95	3.68	3.08	1.74	0.62
Nd	3.89	4.38	2.85	7.82	4.02	3.57	14.44	11.42	6.69	2.43
Sm	0.82	1.00	0.57	1.37	0.94	0.93	2.53	1.79	1.21	0.60
Eu	0.18	0.24	0.10	0.18	0.17	0.25	0.27	0.28	0.20	0.12
Gd	0.91	1.21	0.61	1.06	1.01	1.46	1.68	1.32	0.99	0.66
Tb	0.14	0.19	0.11	0.16	0.16	0.24	0.23	0.21	0.16	0.11
Dy	0.83	1.15	0.71	0.95	0.95	1.40	1.32	1.34	0.91	0.63
Ho	0.18	0.25	0.16	0.20	0.20	0.30	0.28	0.31	0.19	0.13
Er	0.48	0.69	0.48	0.61	0.59	0.85	0.81	0.97	0.55	0.37
Tm	0.07	0.11	0.07	0.10	0.09	0.13	0.12	0.16	0.08	0.05
Yb	0.38	0.67	0.49	0.68	0.62	0.86	0.79	1.12	0.57	0.37
Lu	0.05	0.10	0.07	0.11	0.10	0.13	0.12	0.18	0.09	0.05
Hf	0.44	2.74	2.09	4.57	3.78	3.60	3.18	5.90	3.20	1.62
Ta	0.05	0.19	0.15	0.19	0.24	0.23	0.18	0.20	0.12	0.07
W	0.36	0.61	0.77	1.24	2.93	0.69	0.79	1.47	0.84	0.42
Tl	0.07	0.19	0.08	0.14	0.14	0.25	0.24	0.25	0.10	0.38
Pb	4.01	7.01	11.83	13.45	6.00	3.07	19.35	13.08	4.99	7.76
Th	0.88	2.26	2.14	3.47	2.57	3.47	4.18	5.08	2.96	1.26
U	1.64	1.01	0.73	2.58	2.35	0.98	0.90	2.81	1.01	1.38
Eu/Eu*	0.65	0.66	0.50	0.46	0.53	0.66	0.39	0.55	0.56	0.56
La(N)/Sm(N)	3.31	2.85	3.45	3.91	2.79	2.88	2.82	4.03	3.67	2.55
La(N)/Yb(N)	7.90	4.68	4.47	8.64	4.67	3.43	10.01	7.11	8.54	4.64
Gd(N)/Yb(N)	1.97	1.48	1.03	1.28	1.34	1.40	1.77	0.97	1.43	1.48
CIA	1	72	54	14	14	68	71	69	4	4
PIA	1	92	58	10	10	86	89	88	3	2

	Johnnie Fm. sandstones									
Sample	J17AR	J18AR	J19AR	J20AR	J21A	J22A	J23A	J24A	J25A	J27A
Unit	3	3	3	3	4	4	4	4	4	4
SiO_2	41.91	48.21	36.64	82.53	91.50	90.06	92.30	94.50	94.77	81.06
TiO_2	0.30	0.34	0.21	1.25	1.17	1.46	0.67	0.67	0.35	0.21
Al_2O_3	0.41	1.02	0.90	6.19	2.11	3.03	1.74	1.73	1.87	1.97

(continued on next page)

Table 1 (*continued*)

	Johnnie Fm. sandstones									
Sample	J17AR	J18AR	J19AR	J20AR	J21A	J22A	J23A	J24A	J25A	J27A
Unit	3	3	3	3	4	4	4	4	4	4
FeO(t)	1.01	1.46	1.14	1.32	0.22	0.28	0.39	0.63	0.34	1.63
Fe_2O_3	1.12	1.62	1.27	1.47	0.24	0.32	0.44	0.70	0.38	1.81
MnO	0.12	0.14	0.12	0.03	0.00	0.00	0.00	0.00	0.00	0.10
MgO	11.56	9.34	12.84	1.00	0.05	0.15		0.03	0.01	2.58
CaO	17.46	14.08	20.00	1.07	0.33	0.10	0.00	0.00	0.07	7.32
Na_2O	0.09	0.11	0.11	0.13	0.10	0.07	0.03	0.07	0.02	0.45
K_2O	0.11	0.25	0.26	3.39	0.83	1.44	0.91	0.92	0.90	1.02
P_2O_5	0.03	0.04	0.04	0.19	0.04	0.04	0.04	0.10	0.04	0.29
LOI	26.54	22.33	29.49	2.49	1.11	1.08	0.81	0.68	0.60	3.63
Total	100.67	98.92	103.00	101.06	97.70	98.04	97.32	100.02	99.36	102.07
Li	2.08	2.80	3.35	6.82	1.87	2.63	1.58	1.52	1.32	2.85
Be	0.16	0.23	0.33	0.62	0.12	0.27	0.19	0.18	0.17	0.23
Sc	3.01	3.15	5.05	5.80	2.10	2.87	2.05	1.57	1.23	2.15
Ti	1596.36	1865.40	1168.75	7303.83	6969.02	6907.37	3404.88	3828.13	1707.13	969.29
V	16.01	17.85	24.35	29.67	24.37	22.42	10.65	14.13	7.59	6.41
Cr	3.83	6.32	5.51	15.99	14.18	9.74	6.46	7.74	6.04	4.11
Co	3.81	3.54	3.68	6.27	0.33	0.26	0.22	0.43	0.42	1.69
Ni	5.62	6.46	7.05	8.49	0.44	0.42	0.18	0.33	0.59	4.28
Cu	7.77	12.08	8.76	13.57	5.44	4.70	3.78	3.95	7.19	5.77
Zn	10.52	29.04	25.19	93.42	0.18	0.97	1.18	0.25	1.25	7.53
Ga	0.57	1.16	1.08	6.46	1.43	3.26	1.52	1.65	1.80	2.34
As	6.13	10.91	36.88	20.09	2.40	3.39	4.75	9.72	5.81	10.09
Rb	3.91	8.62	8.02	75.21	15.04	28.40	17.91	20.27	18.26	21.00
Sr	66.31	53.47	153.76	79.52	43.50	52.37	32.77	34.13	35.95	114.91
Y	5.99	8.03	9.56	20.47	7.73	14.56	13.42	10.21	9.67	7.09
Zr	29.60	62.32	43.33	328.08	115.79	371.07	335.80	343.30	262.03	42.49
Nb	1.48	2.02	1.60	11.02	5.47	7.62	5.61	5.55	3.32	1.69
Mo	0.42	0.79	1.04	0.47	0.15	2.21	0.55	1.25	0.46	1.14
Cd	0.17	0.13	0.30	0.20	0.05	0.12	0.12	0.13	0.10	0.04
Sn	0.19	0.24	0.33	0.96	0.45	1.60	0.13	0.39	0.35	0.17
Sb	0.32	0.45	4.65	1.48	0.34	0.70	0.43	1.27	0.63	0.59
Cs	0.13	0.28	0.25	1.33	0.69	0.71	0.43	0.33	0.33	0.48
Ba	19.44	46.19	29.25	694.92	146.05	178.61	126.64	139.11	127.51	138.45
La	3.35	3.80	4.21	25.10	14.12	20.00	13.31	14.52	9.53	9.83
Ce	9.21	9.40	11.37	56.49	28.00	44.73	31.88	35.27	24.06	22.18
Pr	0.94	1.02	1.14	6.11	3.28	4.81	3.26	3.74	2.74	2.42
Nd	3.84	4.26	4.77	22.45	12.12	17.39	11.75	14.07	11.23	9.25
Sm	1.05	1.41	1.37	4.26	2.31	3.17	2.13	2.67	2.39	1.83
Eu	0.23	0.33	0.27	0.72	0.31	0.56	0.48	0.43	0.40	0.43
Gd	1.15	1.70	1.57	3.74	1.77	2.94	2.40	2.23	2.03	1.72
Tb	0.19	0.26	0.26	0.61	0.24	0.44	0.39	0.33	0.30	0.25
Dy	1.11	1.54	1.62	3.69	1.41	2.60	2.40	1.92	1.74	1.36
Ho	0.23	0.31	0.34	0.79	0.30	0.55	0.50	0.40	0.37	0.27
Er	0.63	0.83	0.96	2.23	0.82	1.60	1.44	1.14	1.05	0.69
Tm	0.09	0.12	0.14	0.34	0.12	0.25	0.23	0.18	0.17	0.10
Yb	0.60	0.80	0.92	2.26	0.78	1.71	1.48	1.21	1.10	0.61
Lu	0.09	0.12	0.13	0.34	0.12	0.27	0.23	0.19	0.18	0.09
Hf	0.72	1.48	1.06	8.08	3.02	9.77	8.09	8.40	6.41	1.16
Ta	0.08	0.11	0.08	0.50	0.35	0.47	0.36	0.35	0.23	0.11
W	0.61	1.37	4.21	3.37	2.19	2.39	0.98	1.36	0.89	0.79
Tl	0.10	0.42	0.12	0.52	0.12	0.19	0.13	0.12	0.15	1.42
Pb	9.70	4.82	302.51	15.91	3.17	5.35	4.53	7.41	4.23	5.41
Th	1.63	2.22	2.35	9.92	6.24	7.15	5.07	5.36	2.72	1.61
U	1.31	1.42	1.05	1.75	0.86	1.60	1.20	1.55	1.31	0.85
Eu/Eu*	0.62	0.64	0.56	0.55	0.47	0.55	0.64	0.53	0.55	0.73
La(N)/Sm(N)	2.01	1.69	1.92	3.70	3.83	3.95	3.92	3.40	2.50	3.36
La(N)/Yb(N)	3.84	3.28	3.16	7.68	12.51	8.11	6.24	8.33	6.00	11.18
Gd(N)/Yb(N)	1.57	1.75	1.41	1.37	1.87	1.42	1.35	1.53	1.52	2.33
CIA	1	4	2	54	57	63	62	61	64	12
PIA	1	3	2	60	64	88	93	86	93	6

	Johnnie Fm. sandstones						
Sample	J29A	J33A	J36A	J39A	J43AR	J44A	J45A
Unit	4	4	4	4	5	5	5
SiO_2	85.12	79.17	95.20	96.29	63.09	79.41	70.51
TiO_2	0.47	0.64	0.05	0.07	0.72	0.42	0.68
Al_2O_3	8.29	6.78	0.84	0.56	9.85	8.84	14.26
FeO(t)	1.10	3.23	0.01		6.84	3.98	2.56
Fe_2O_3	1.22	3.59	0.01		7.60	4.42	2.84
MnO	0.00	0.04	0.00	0.00	0.25	0.02	0.01
MgO	0.44	0.62	0.00		0.54	0.25	0.96
CaO	0.20	2.24	0.00	0.04	6.94	0.00	1.98

Table 1 (*continued*)

	Johnnie Fm. sandstones						
Sample	J29A	J33A	J36A	J39A	J43AR	J44A	J45A
Unit	4	4	4	4	5	5	5
Na_2O	0.40	0.54	0.04	0.00	1.44	1.87	1.72
K_2O	3.30	3.10	0.27	0.14	2.18	0.95	2.64
P_2O_5	0.05	0.58	0.04	0.02	0.24	0.03	0.07
LOI	0.90	2.02	0.30	0.21	7.85	2.13	2.36
Total	101.49	102.53	96.77	97.33	107.55	102.33	100.59
Li	7.23	8.99	2.69	2.73	14.11	306.44	33.17
Be	0.78	0.85	0.10	0.10	1.38	1.12	1.73
Sc	3.43	4.71	0.34	0.25	18.31	5.96	9.05
Ti	2789.09	3668.51	325.84	489.71	4235.54	2293.82	3793.57
V	32.70	19.92	2.44	2.28	51.57	23.10	43.10
Cr	35.30	25.67	2.18	3.27	50.79	28.71	50.93
Co	1.26	4.01	0.38	0.10	8.72	4.62	2.53
Ni	2.83	8.68	0.52	0.50	28.67	14.86	12.22
Cu	7.59	11.56	4.83	6.79	20.91	11.63	16.02
Zn	25.10	20.21	8.97	7.27	23.95	47.93	43.17
Ga	9.52	8.23	0.85	0.60	12.23	8.60	14.43
As	4.43	4.79	0.86	1.16	56.70	4.38	6.47
Rb	80.21	74.31	6.08	3.30	71.70	29.43	81.74
Sr	48.18	73.28	4.90	4.94	144.75	87.44	62.41
Y	11.03	20.91	2.71	3.05	47.19	19.87	29.98
Zr	164.69	486.39	47.93	80.80	698.50	457.29	530.28
Nb	7.77	8.13	0.70	1.06	12.96	6.67	12.20
Mo	0.48	1.75	0.16	0.14	1.70	0.44	0.44
Cd	0.14	0.21	0.04	0.04	0.32	0.17	0.19
Sn	1.81	0.87	0.42	0.19	0.04	0.63	2.37
Sb	0.33	0.22	0.10	0.16	0.34	0.15	0.19
Cs	1.72	1.48	0.24	0.20	2.18	4.56	3.73
Ba	341.93	372.61	30.69	17.41	285.38	102.14	274.37
La	19.65	28.41	5.61	5.55	40.52	14.61	29.04
Ce	40.81	70.39	12.35	11.41	93.59	31.00	63.26
Pr	4.72	6.99	1.40	1.33	10.72	3.52	7.32
Nd	17.24	25.90	5.11	4.78	41.11	12.48	27.54
Sm	2.85	4.95	0.80	0.72	8.62	2.39	5.27
Eu	0.44	0.84	0.10	0.07	1.87	0.49	0.99
Gd	1.97	4.51	0.58	0.60	9.02	2.74	5.18
Tb	0.31	0.69	0.09	0.09	1.44	0.52	0.85
Dy	1.96	3.97	0.51	0.54	8.36	3.41	5.16
Ho	0.44	0.82	0.11	0.11	1.69	0.75	1.10
Er	1.25	2.36	0.31	0.31	4.73	2.19	3.17
Tm	0.19	0.37	0.05	0.05	0.73	0.35	0.50
Yb	1.25	2.51	0.33	0.32	4.90	2.32	3.34
Lu	0.19	0.39	0.05	0.05	0.75	0.37	0.52
Hf	4.38	12.20	1.27	1.91	16.93	11.39	13.30
Ta	0.56	0.59	0.05	0.13	0.90	0.49	0.87
W	1.04	1.88	0.22	0.26	1.30	0.89	1.20
Tl	0.41	0.99	0.04	0.02	0.42	0.16	0.39
Pb	11.49	11.29	0.92	1.15	28.48	6.79	11.56
Th	5.31	10.63	1.29	1.80	15.04	7.02	11.30
U	1.51	3.26	0.43	0.55	5.40	2.61	2.90
Eu/Eu*	0.56	0.54	0.44	0.34	0.64	0.58	0.58
La(N)/Sm(N)	4.33	3.60	4.38	4.81	2.95	3.84	3.45
La(N)/Yb(N)	10.89	7.83	11.94	12.03	5.73	4.37	6.01
Gd(N)/Yb(N)	1.31	1.48	1.48	1.54	1.52	0.98	1.28
CIA	65	50	70	77	37	68	61
PIA	84	49	89	97	34	72	65

	Johnnie Fm. sandstones								
Sample	J56A	J58A	J59A	J65AR	J66AR	J67A	J68A	J70A	J74A
Unit	6	6	6	6	6	6	7	7	7
SiO_2	56.67	81.00	64.99	84.02	80.64	78.03	75.63	83.63	81.48
TiO_2	0.45	0.29	0.96	0.40	0.51	0.38	0.38	0.10	0.10
Al_2O_3	9.90	8.48	13.53	7.84	9.60	8.78	9.73	7.45	9.17
FeO(t)	4.12	2.13	7.83	0.60	1.37	2.16	1.84	0.27	0.47
Fe_2O_3	4.58	2.37	8.70	0.66	1.53	2.40	2.04	0.30	0.52
MnO	0.10	0.02	0.02	0.01	0.00	0.01	0.01	0.01	0.00
MgO	4.42	0.54	4.01	0.19	0.75	1.31	1.94	0.36	0.21
CaO	10.74	0.38	0.24	0.09	0.04	0.34	0.08	0.54	0.22
Na_2O	1.45	1.55	1.68	2.29	2.26	1.97	1.04	1.92	2.88
K_2O	3.35	3.23	3.56	3.16	3.70	3.28	4.19	3.43	3.07
P_2O_5	0.22	0.15	0.09	0.03	0.03	0.05	0.03	0.05	0.02
LOI	7.71	0.84	2.81	0.70	0.98	1.51	1.82	1.21	0.84

(*continued on next page*)

Table 1 (*continued*)

	Johnnie Fm. sandstones								
Sample	J56A	J58A	J59A	J65AR	J66AR	J67A	J68A	J70A	J74A
Unit	6	6	6	6	6	6	7	7	7
TOTAL	103.72	100.96	108.41	99.99	101.41	100.21	98.72	99.26	98.99
Li	29.78	23.67	85.94	5.69	17.34	20.36	32.16	2.49	5.69
Be	1.45	1.00	2.28	0.48	0.94	0.50	0.92	0.23	0.50
Sc	7.86	5.80	14.73	3.68	3.10	4.87	4.56	1.22	1.71
Ti	2493.37	1531.64	5913.30	2366.86	2797.21	2241.77	2051.03	616.78	516.17
V	29.95	23.41	75.67	14.82	26.94	21.46	22.31	2.83	6.46
Cr	34.78	24.59	90.20	28.27	34.93	31.51	31.14	8.74	7.99
Co	4.54	4.03	9.71	0.89	2.00	1.98	7.33	0.42	2.67
Ni	13.52	11.65	28.01	2.27	6.86	6.13	19.91	0.70	0.99
Cu	9.18	9.55	12.88	5.63	23.20	6.14	9.64	4.35	9.62
Zn	48.47	217.98	91.42	7.12	20.70	18.24	38.00	3.00	4.13
Ga	11.40	10.20	21.93	6.27	10.15	9.16	9.70	5.10	5.79
As	3.86	2.07	4.24	4.12	1.92	2.25	0.97	0.54	1.50
Rb	101.46	79.47	114.29	67.91	67.66	71.07	108.15	69.86	58.35
Sr	100.61	75.18	62.15	54.65	57.31	64.20	50.62	56.96	47.17
Y	21.31	17.58	26.21	18.81	13.24	17.68	12.69	6.25	5.78
Zr	168.30	132.77	297.02	433.80	369.54	347.90	160.47	34.15	43.29
Nb	10.48	7.35	22.91	8.18	10.19	8.50	8.42	3.06	2.62
Mo	0.54	0.28	0.16	0.72	0.12	0.39	0.07	0.18	0.17
Cd	0.09	0.10	0.10	0.18	0.13	0.12	0.07	0.03	0.02
Sn	1.26	0.97	0.41	0.72	1.05	0.86	1.45	0.41	0.43
Sb	0.14	0.11	0.16	0.11	0.13	0.08	0.11	0.06	0.14
Cs	2.47	1.87	3.06	0.96	1.49	1.03	3.34	0.83	1.04
Ba	461.46	568.73	575.54	672.00	760.21	786.91	612.81	1006.82	437.61
La	22.76	26.75	34.08	18.89	19.52	14.62	18.27	10.23	9.50
Ce	51.49	71.01	75.27	42.36	47.65	42.88	38.74	26.07	23.63
Pr	6.02	7.29	8.44	4.68	5.63	4.88	4.37	2.54	2.30
Nd	23.32	28.24	30.83	17.40	21.58	19.73	16.45	9.71	8.43
Sm	4.98	6.47	4.99	3.61	4.04	3.98	3.19	2.00	1.40
Eu	1.10	1.13	1.12	0.81	0.63	0.71	0.55	0.44	0.31
Gd	4.66	5.97	4.33	3.22	2.80	3.19	2.40	1.61	1.23
Tb	0.70	0.80	0.75	0.53	0.42	0.52	0.36	0.23	0.19
Dy	3.97	4.06	4.67	3.23	2.52	3.28	2.28	1.29	1.14
Ho	0.80	0.75	1.01	0.67	0.55	0.69	0.50	0.26	0.23
Er	2.22	1.92	2.94	1.95	1.66	1.88	1.48	0.69	0.63
Tm	0.34	0.27	0.46	0.30	0.27	0.28	0.24	0.10	0.10
Yb	2.20	1.71	3.05	2.10	1.85	1.82	1.64	0.65	0.62
Lu	0.33	0.25	0.46	0.32	0.29	0.28	0.25	0.10	0.09
Hf	4.37	3.43	7.77	10.30	9.66	8.47	4.08	0.96	1.12
Ta	0.69	0.53	1.50	0.55	0.71	0.60	0.56	0.21	0.18
W	0.90	0.48	1.32	0.70	0.74	0.62	0.81	0.25	0.28
Tl	0.52	0.40	0.50	0.35	0.42	0.37	0.44	0.35	0.28
Pb	7.36	10.64	11.58	8.81	9.56	8.03	7.34	8.01	8.68
Th	6.81	5.45	12.55	7.58	7.95	7.17	5.62	2.03	1.75
U	1.83	1.18	2.64	1.59	1.53	1.49	1.01	0.55	0.70
Eu/Eu*	0.69	0.55	0.73	0.72	0.57	0.61	0.60	0.75	0.72
La(N)/Sm(N)	2.86	2.59	4.28	3.28	3.03	2.30	3.58	3.21	4.25
La(N)/Yb(N)	7.16	10.84	7.74	6.23	7.31	5.57	7.69	10.88	10.68
Gd(N)/Yb(N)	1.75	2.89	1.18	1.27	1.25	1.45	1.21	2.04	1.65
CIA	28	57	66	52	55	55	61	49	52
PIA	23	63	77	53	60	58	74	48	54

	Johnnie Fm Sandstones	Johnnie Fm. mudstones						
Sample	J94AR	J2B	J7B	J10B	J11B	J12B	J13BR	J14B	J17BR
Unit	8	2	2	2	2	2	2	2	3
SiO_2	87.13	73.92	65.24	61.11	67.79	55.91	60.69	73.27	27.61
TiO_2	0.02	1.47	1.20	3.03	1.37	1.60	5.48	1.59	0.42
Al_2O_3	0.31	12.63	17.64	19.36	14.85	21.06	11.99	11.56	8.50
FeO(t)	2.52	2.88	3.28	3.87	5.53	6.40	9.04	3.68	3.55
Fe_2O_3	2.81	3.20	3.65	4.30	6.15	7.12	10.05	4.09	3.95
MnO	0.11	0.00	0.01	0.02	0.03	0.03	0.02	0.01	0.07
MgO	0.85	1.14	1.37	1.69	1.36	2.05	1.53	1.24	11.13
CaO	3.59	0.80	0.00	0.28	0.27	0.16	1.29	0.11	15.57
Na_2O	0.09	0.09	0.06	0.12	0.06	0.15	0.06	0.10	0.17
K_2O	0.06	4.47	6.06	6.90	5.21	7.65	4.16	4.08	2.99
P_2O_5	0.04	0.06	0.07	0.22	0.14	0.04	0.12	0.04	0.08
LOI	4.70	3.21	3.40	3.94	3.54	4.69	3.34	2.58	26.22
Total	102.23	103.85	101.99	104.85	106.30	106.86	107.78	102.35	100.25
Li	2.47	12.05	16.00	20.64	17.29	19.46	12.33	16.73	19.81
Be	0.12	1.34	1.28	1.65	1.58	2.17	1.28	1.33	0.88
Sc	0.74	13.69	10.08	15.55	19.40	21.86	10.39	8.74	12.75
Ti	165.89	8595.56	7100.13	15598.12	8180.39	9368.96	30217.92	8840.63	2429.84

Table 1 (*continued*)

	Johnnie Fm Sandstones	Johnnie Fm. mudstones							
Sample	J94AR	J2B	J7B	J10B	J11B	J12B	J13BR	J14B	J17BR
Unit	8	2	2	2	2	2	2	2	3
V	4.80	136.54	208.47	231.71	136.27	207.29	170.76	253.84	82.11
Cr	2.49	52.14	39.12	83.52	69.95	120.08	79.89	63.95	41.03
Co	1.11	8.89	4.66	10.62	24.94	24.98	11.28	13.18	11.18
Ni	2.84	24.04	7.26	14.31	43.15	46.29	13.32	23.17	21.55
Cu	10.03	20.74	17.45	15.77	35.27	36.05	44.89	82.22	26.98
Zn	78.50	8.76	5.86	7.71	10.70	17.76	36.93	12.17	19.85
Ga	0.82	15.33	15.21	20.66	21.69	29.99	12.96	15.53	11.08
As	2.61	14.44	22.32	35.96	25.65	47.28	37.21	33.22	30.15
Rb	3.65	113.04	139.10	156.52	137.35	197.32	103.29	104.20	92.62
Sr	42.24	50.29	72.77	15.64	312.95	29.13	56.21	14.92	141.97
Y	6.37	24.36	18.68	34.87	32.14	45.17	54.08	15.64	16.70
Zr	25.13	293.34	340.90	533.38	254.53	341.15	1481.14	323.11	108.39
Nb	0.44	12.81	10.17	20.44	14.29	23.63	41.50	13.57	7.49
Mo	1.29	1.31	4.23	2.15	2.42	1.62	8.29	3.44	1.35
Cd	0.20	0.12	0.13	0.21	0.14	0.18	0.60	0.15	0.22
Sn	0.09	2.14	1.58	2.01	2.69	4.47	0.17	2.61	2.12
Sb	0.17	0.77	1.56	0.48	1.10	0.98	3.48	3.74	2.15
Cs	0.20	4.08	4.97	5.53	4.97	7.77	6.34	3.23	2.82
Ba	43.32	246.79	366.67	335.58	289.13	385.63	255.07	262.05	198.30
La	4.48	35.48	24.52	35.71	41.05	73.71	85.72	55.21	24.21
Ce	12.37	77.48	51.23	69.19	91.19	129.77	166.57	107.31	54.15
Pr	1.42	9.08	5.80	7.46	10.99	13.06	18.34	9.92	6.18
Nd	5.78	33.05	21.04	26.36	41.55	44.21	62.42	33.15	22.46
Sm	1.44	5.54	3.74	4.61	6.84	7.05	8.98	3.60	3.82
Eu	0.31	1.19	0.83	1.05	1.41	1.42	1.20	0.50	0.52
Gd	1.49	4.25	3.02	4.40	5.69	6.12	6.26	1.87	2.74
Tb	0.24	0.66	0.48	0.76	0.91	1.13	1.21	0.34	0.47
Dy	1.31	4.13	3.12	5.30	5.61	7.51	8.76	2.45	3.01
Ho	0.25	0.90	0.69	1.26	1.22	1.68	2.09	0.61	0.67
Er	0.63	2.59	2.08	4.07	3.48	4.87	6.54	1.99	1.99
Tm	0.09	0.40	0.34	0.68	0.53	0.75	1.07	0.35	0.32
Yb	0.54	2.56	2.27	4.70	3.40	4.84	7.23	2.39	2.11
Lu	0.08	0.39	0.35	0.75	0.52	0.74	1.12	0.39	0.31
Hf	0.73	7.61	8.50	16.77	6.62	9.31	40.76	8.54	2.95
Ta	0.04	0.80	0.64	1.27	0.92	1.63	3.67	0.92	0.56
W	0.17	1.94	3.24	3.10	2.41	2.71	10.98	2.75	2.87
Tl	0.05	0.76	1.06	1.24	1.02	2.34	1.12	0.84	0.55
Pb	4.06	12.93	17.83	19.80	18.32	22.23	81.83	22.66	48.63
Th	1.35	9.26	7.16	15.28	13.11	27.12	83.52	12.58	10.57
U	1.77	3.26	12.21	9.04	3.17	4.62	9.99	5.69	2.82
Eu/Eu*	0.65	0.75	0.75	0.71	0.69	0.66	0.49	0.59	0.45
La(N)/Sm(N)	1.95	4.02	4.11	4.86	3.76	6.56	5.98	9.62	3.98
La(N)/Yb(N)	5.77	9.60	7.47	5.26	8.37	10.54	8.20	15.97	7.93
Gd(N)/Yb(N)	2.29	1.37	1.10	0.77	1.38	1.04	0.71	0.65	1.25
CIA	4	67	73	72	72	71	64	71	21
PIA	4	84	99	98	97	97	78	96	16

	Johnnie Fm. mudstones							
Sample	J18B	J19BR	J29B	J42B	J43B	J45B	J47B	J49B
Unit	3	3	4	5	5	5	5	5
SiO_2	59.64	23.56	73.40	60.91	63.61	62.06	65.18	70.48
TiO_2	0.94	0.37	0.88	0.91	1.13	1.01	0.96	1.08
Al_2O_3	18.65	6.88	14.73	17.65	19.21	20.07	17.03	16.19
FeO(t)	5.17	3.24	0.76	9.31	4.85	5.67	5.64	3.28
Fe_2O_3	5.75	3.60	0.85	10.34	5.39	6.30	6.26	3.64
MnO	0.00	0.10	0.01	0.01	0.00	0.01	0.05	0.01
MgO	2.03	12.65	0.84	0.85	0.83	1.57	0.68	1.20
CaO	0.01	19.04	1.13	0.05	0.17	0.19	0.63	0.20
Na_2O	0.10	0.15	0.33	0.80	1.23	0.82	1.60	1.74
K_2O	6.92	2.31	5.63	4.44	5.11	5.30	4.43	4.49
P_2O_5	0.08	0.08	0.08	0.50	0.03	0.15	0.06	0.07
LOI	4.01	30.09	2.10	4.78	3.10	3.66	3.56	2.48
Total	103.30	102.09	100.74	110.56	104.67	106.81	106.06	104.85
Li	33.67	12.62	14.50	32.55	25.74	62.03	65.98	28.80
Be	2.86	0.90	1.43	2.79	2.62	3.37	2.58	2.33
Sc	20.88	8.40	11.32	17.21	9.09	13.88	9.97	7.50
Ti	5334.17	2146.27	5450.72	5528.44	6654.37	5902.50	5436.64	6661.09
V	171.34	61.14	69.75	105.57	94.57	89.42	84.98	83.73
Cr	97.24	34.47	69.45	98.39	103.09	98.50	85.16	71.92
Co	12.29	9.77	0.76	5.24	2.22	3.03	8.52	5.59
Ni	24.34	18.29	2.00	18.93	7.72	24.12	17.68	18.73

(*continued on next page*)

Table 1 (*continued*)

	Johnnie Fm. mudstones							
Sample	J18B	J19BR	J29B	J42B	J43B	J45B	J47B	J49B
Unit	3	3	4	5	5	5	5	5
Cu	51.37	17.49	5.74	24.66	29.34	52.28	16.74	16.45
Zn	32.71	34.69	17.75	44.55	22.54	76.87	74.83	51.41
Ga	27.04	9.15	19.58	24.57	24.65	27.20	22.19	21.42
As	145.84	45.62	3.60	56.08	18.18	8.56	5.72	18.99
Rb	200.96	72.35	144.18	148.41	142.47	147.24	119.06	118.16
Sr	21.25	162.60	49.05	85.30	98.69	60.47	76.43	48.61
Y	33.12	16.43	16.61	35.80	24.46	29.43	22.58	31.32
Zr	132.26	104.66	315.71	328.19	340.11	385.99	316.37	857.62
Nb	13.47	6.90	16.68	18.97	24.42	20.47	19.16	22.31
Mo	1.17	1.27	0.33	0.99	0.94	0.68	0.54	0.83
Cd	0.10	0.25	0.14	0.12	0.13	0.16	0.14	0.32
Sn	4.64	1.63	3.93	0.35	3.45	3.45	2.91	2.98
Sb	3.43	4.21	0.22	0.51	0.48	8.49	0.30	0.25
Cs	6.85	2.15	3.23	5.03	4.60	7.05	4.34	4.66
Ba	518.74	149.52	584.01	515.67	469.81	549.57	505.79	465.05
La	66.82	31.47	34.92	52.98	44.66	52.19	41.63	42.91
Ce	127.56	63.10	74.44	106.57	93.14	108.65	89.55	96.86
Pr	15.42	7.21	8.85	13.13	10.99	13.16	10.75	10.84
Nd	54.86	25.60	33.50	48.33	39.93	48.67	40.21	40.63
Sm	9.04	4.15	6.32	9.11	6.82	8.91	7.27	7.69
Eu	1.35	0.57	0.91	1.64	1.20	1.75	1.27	1.32
Gd	6.14	2.98	3.93	7.29	5.01	6.98	5.02	5.88
Tb	0.97	0.49	0.54	1.11	0.78	1.06	0.76	0.95
Dy	6.02	2.99	3.14	6.64	4.90	6.12	4.60	6.01
Ho	1.28	0.64	0.66	1.38	1.06	1.25	0.98	1.33
Er	3.74	1.86	1.90	4.07	3.17	3.56	2.93	4.06
Tm	0.56	0.29	0.30	0.63	0.50	0.55	0.47	0.67
Yb	3.60	1.89	2.01	4.10	3.40	3.69	3.19	4.65
Lu	0.53	0.28	0.31	0.61	0.51	0.57	0.49	0.74
Hf	3.80	2.84	8.29	9.02	9.27	10.63	9.43	22.85
Ta	1.00	0.49	1.21	1.35	1.62	1.48	1.38	1.61
W	2.75	5.61	1.64	1.71	1.75	1.67	1.54	1.63
Tl	1.11	0.45	0.79	0.73	0.74	0.78	0.63	0.65
Pb	16.52	570.54	17.32	32.30	36.34	20.62	11.98	11.48
Th	16.34	9.28	10.61	16.51	14.72	15.71	12.72	16.57
U	4.66	2.54	2.39	5.66	3.69	4.69	3.37	4.86
Eu/Eu*	0.55	0.46	0.56	0.61	0.63	0.67	0.64	0.60
La(N)/Sm(N)	4.63	4.76	3.46	3.65	4.10	3.67	3.59	3.50
La(N)/Yb(N)	12.83	11.56	12.01	8.95	9.10	9.79	9.04	6.39
Gd(N)/Yb(N)	1.41	1.48	1.62	1.47	1.22	1.56	1.30	1.05
CIA	71	16	63	74	71	74	67	67
PIA	98	11	78	91	86	91	77	79

	Johnnie Fm. mudstones									
Sample	J56B	J57B	J58B	J59B	J68B	J70B	J71B	J72B	J74B	J77B
Unit	6	6	6	6	7	7	7	7	7	7
SiO_2	57.87	53.89	73.06	66.40	63.78	59.47	87.88	60.37	52.78	70.88
TiO_2	0.61	0.70	0.35	0.75	0.71	0.18	0.10	0.67	0.92	0.90
Al_2O_3	12.49	11.69	9.76	13.40	16.50	8.02	5.69	16.91	21.25	13.65
FeO(t)	4.49	5.11	4.47	6.86	5.67	1.94	0.24	5.74	7.63	4.87
Fe_2O_3	4.98	5.68	4.97	7.63	6.30	2.15	0.27	6.38	8.48	5.41
MnO	0.08	0.08	0.03	0.02	0.01	0.04	0.00	0.01	0.01	0.01
MgO	3.82	4.50	1.64	2.74	3.80	6.87	0.24	4.81	2.28	2.18
CaO	8.52	8.07	0.76	0.47	0.00	10.24	0.29	0.06	0.41	0.06
Na_2O	0.99	1.69	1.63	1.46	0.48	1.83	1.00	0.88	0.32	1.43
K_2O	4.44	3.81	3.81	4.45	6.79	3.11	3.34	5.55	8.73	4.18
P_2O_5	0.36	0.21	0.36	0.27	0.06	0.08	0.07	0.07	0.07	0.08
LOI	6.37	10.02	1.97	2.50	3.60	5.15	0.83	3.97	3.22	2.76
Total	105.02	105.45	102.82	106.95	107.67	99.08	99.94	105.41	106.11	106.40
Li	43.57	49.39	43.62	72.77	83.81	13.80	3.02	90.57	72.95	49.53
Be	2.03	2.42	1.73	3.13	2.31	0.99	0.29	2.81	4.87	2.33
Sc	10.94	11.86	11.42	12.17	14.29	3.65	1.61	11.54	17.80	13.51
Ti	3423.35	4545.81	2400.64	4879.77	4101.82	925.22	523.88	3685.30	5390.03	5349.23
V	48.33	54.85	36.84	57.52	80.71	15.66	5.41	58.73	95.49	61.31
Cr	56.67	68.25	36.54	67.17	75.32	18.14	8.55	70.53	102.07	63.33
Co	7.47	6.13	7.33	14.47	12.28	3.02	0.55	4.24	15.03	6.53
Ni	20.95	20.21	21.47	23.59	39.85	5.61	1.02	35.60	38.84	19.94
Cu	16.02	14.06	24.68	21.77	3.03	3.93	6.93	5.85	5.51	14.22
Zn	44.59	53.73	104.82	60.98	71.86	16.38	3.08	98.50	70.25	60.84
Ga	15.53	17.85	14.22	20.39	21.35	8.87	4.82	23.12	32.02	18.70
As	5.76	5.29	4.69	4.34	0.92	1.40	0.69	1.69	2.21	7.50
Rb	134.71	130.41	114.55	146.88	224.01	84.91	72.20	202.00	305.64	123.88

Table 1 (*continued*)

	Johnnie Fm. mudstones									
Sample	J56B	J57B	J58B	J59B	J68B	J70B	J71B	J72B	J74B	J77B
Unit	6	6	6	6	7	7	7	7	7	7
Sr	99.35	119.07	87.92	82.50	30.23	120.55	59.23	38.57	24.04	50.21
Y	28.64	26.65	25.09	31.47	24.56	8.71	5.60	16.42	27.55	33.31
Zr	230.67	275.49	211.70	409.30	168.76	45.06	55.64	125.32	197.31	537.25
Nb	14.29	19.43	11.12	19.11	15.99	4.28	2.28	16.19	28.86	19.55
Mo	0.62	0.47	0.42	0.48	0.04	0.20	0.30	0.12	0.14	0.33
Cd	0.09	0.10	0.11	0.14	0.07	0.06	0.03	0.07	0.08	0.23
Sn	2.11	2.43	1.63	2.75	2.21	0.59	0.34	3.50	3.92	0.90
Sb	0.18	0.22	0.16	0.18	0.29	0.12	0.06	0.19	0.52	0.29
Cs	3.66	3.46	3.19	4.28	6.79	1.52	0.95	4.79	9.51	3.52
Ba	581.01	657.27	679.54	766.38	515.09	441.82	1141.30	785.53	1195.18	703.48
La	35.39	39.30	42.94	43.59	46.70	12.75	10.54	35.17	60.88	33.83
Ce	75.23	92.45	99.64	95.30	90.20	33.75	26.51	78.01	126.02	70.82
Pr	9.23	10.24	10.75	10.99	10.97	3.20	2.55	8.28	13.94	7.50
Nd	34.88	37.94	40.31	42.41	38.56	11.92	9.48	29.16	50.13	27.01
Sm	6.96	6.56	8.17	8.82	6.38	2.27	1.71	4.55	8.36	4.94
Eu	1.44	1.33	1.52	1.69	1.12	0.59	0.41	0.99	1.78	0.90
Gd	6.23	5.38	7.36	7.78	4.82	1.95	1.28	3.47	5.99	4.65
Tb	0.93	0.84	1.05	1.07	0.78	0.30	0.19	0.53	0.94	0.87
Dy	5.29	4.99	5.56	5.84	4.74	1.71	1.10	3.16	5.60	5.77
Ho	1.08	1.05	1.05	1.18	0.99	0.34	0.22	0.67	1.17	1.26
Er	2.97	2.97	2.71	3.32	2.87	0.95	0.62	1.94	3.35	3.76
Tm	0.45	0.46	0.39	0.52	0.45	0.14	0.10	0.31	0.51	0.60
Yb	2.86	3.01	2.42	3.45	2.93	0.91	0.63	2.01	3.33	4.00
Lu	0.42	0.45	0.35	0.53	0.44	0.13	0.09	0.30	0.49	0.62
Hf	5.92	7.00	5.39	10.63	4.67	1.30	1.44	3.49	5.37	16.32
Ta	0.94	1.26	0.76	1.28	1.10	0.29	0.17	1.10	1.97	1.34
W	1.05	1.19	0.74	1.07	1.15	0.47	0.21	1.25	2.27	1.27
Tl	0.60	0.58	0.54	0.66	0.80	0.35	0.36	0.80	1.24	0.54
Pb	10.24	11.51	14.48	16.16	7.31	7.59	6.81	9.00	4.36	18.71
Th	10.09	11.96	8.21	12.78	12.70	3.09	2.08	9.56	14.38	17.39
U	2.57	2.65	1.67	3.16	2.00	1.05	0.56	1.68	2.41	3.43
Eu/Eu*	0.66	0.68	0.59	0.62	0.58	0.85	0.84	0.74	0.73	0.54
La(N)/Sm(N)	3.19	3.76	3.30	3.10	4.58	3.53	3.85	4.84	4.56	4.30
La(N)/Yb(N)	8.57	9.03	12.26	8.74	11.02	9.65	11.61	12.10	12.67	5.86
Gd(N)/Yb(N)	1.80	1.48	2.51	1.86	1.49	1.80	1.68	1.51	1.63	1.09
CIA	37	36	57	64	67	24	50	69	67	66
PIA	32	31	64	77	92	18	51	88	91	79

	Johnnie Fm. mudstones				
Sample	J95B	J96B	J97B	J98B	J99B
Unit	8	8	8	8	8
SiO_2	63.35	64.77	57.72	58.27	62.64
TiO_2	0.81	0.77	0.76	0.89	0.93
Al_2O_3	18.22	18.03	21.70	20.38	19.47
FeO(t)	7.42	6.26	8.04	6.42	6.61
Fe_2O_3	8.25	6.96	8.93	7.14	7.34
MnO	0.02	0.02	0.02	0.06	0.04
MgO	1.95	1.67	1.49	1.77	1.84
CaO	0.02	0.19	0.00	0.08	0.29
Na_2O	0.20	0.39	0.30	0.37	0.30
K_2O	4.41	4.45	4.98	4.72	4.63
P_2O_5	0.06	0.05	0.06	0.08	0.33
LOI	4.69	4.43	4.91	4.57	4.73
Total	109.39	108.00	108.92	104.75	109.14
Li	47.38	42.63	53.26	55.25	53.15
Be	2.76	2.67	2.78	2.60	3.03
Sc	16.94	17.14	18.85	18.35	20.22
Ti	4651.27	4517.49	4434.32	5016.49	5381.36
V	116.84	99.18	117.37	113.95	129.65
Cr	94.58	86.62	103.05	104.30	108.90
Co	11.47	12.33	13.35	15.69	17.93
Ni	37.38	31.88	55.51	35.17	32.96
Cu	44.70	33.69	24.05	38.09	37.21
Zn	96.02	76.00	78.23	186.30	55.03
Ga	23.12	23.00	27.88	27.07	27.02
As	5.09	6.81	9.36	11.83	17.89
Rb	137.22	138.56	173.17	163.63	161.39
Sr	60.94	36.44	61.90	58.54	59.03
Y	37.86	26.08	25.94	27.36	38.38
Zr	296.65	224.45	140.57	246.36	269.43
Nb	14.66	14.11	14.47	16.74	17.06

(*continued on next page*)

Table 1 (*continued*)

	Johnnie Fm. mudstones				
Sample	J95B	J96B	J97B	J98B	J99B
Unit	8	8	8	8	8
Mo	1.07	0.84	0.78	0.87	1.27
Cd	0.15	0.10	0.06	0.20	0.10
Sn	3.02	1.98	0.77	2.50	3.61
Sb	0.21	0.26	0.42	0.36	1.18
Cs	4.10	4.06	4.41	4.46	3.79
Ba	542.03	463.05	567.39	470.82	477.44
La	54.09	43.80	47.47	47.15	56.62
Ce	115.41	93.04	91.97	94.22	120.93
Pr	13.56	10.75	11.12	11.36	13.55
Nd	50.40	39.95	40.34	41.76	50.05
Sm	9.31	7.41	7.14	7.63	9.12
Eu	1.86	1.33	1.38	1.47	1.71
Gd	8.03	5.60	5.50	6.06	7.69
Tb	1.24	0.84	0.84	0.91	1.21
Dy	7.15	4.89	4.95	5.26	7.22
Ho	1.47	1.01	1.02	1.08	1.49
Er	4.10	2.86	2.89	3.02	4.17
Tm	0.61	0.43	0.44	0.46	0.63
Yb	3.85	2.80	2.80	2.95	4.00
Lu	0.57	0.42	0.41	0.44	0.60
Hf	8.13	5.95	3.88	6.60	7.55
Ta	1.10	1.05	1.06	1.23	1.25
W	1.53	1.36	1.37	1.47	1.78
Tl	0.68	0.68	0.87	0.82	0.79
Pb	8.76	10.64	11.58	10.19	50.04
Th	17.70	14.97	15.69	17.45	17.85
U	4.15	3.29	4.18	3.73	4.11
Eu/Eu*	0.65	0.63	0.67	0.66	0.62
La(N)/Sm(N)	3.64	3.71	4.17	3.87	3.89
La(N)/Yb(N)	9.72	10.85	11.75	11.07	9.80
Gd(N)/Yb(N)	1.72	1.66	1.63	1.70	1.59
CIA	78	76	79	78	78
PIA	98	94	97	96	97

upper crust (Nesbitt and Markovics, 1997). Sandstone from Units 2 and 4 exhibit high ratios (Zr/Sc≥100) suggesting that they have gone through several sedimentary cycles (cf., McLennan, et al., 1993).

5. Sediment composition evolution

Geochemical trends, paleoweathering, and provenance interpretations can only be addressed after samples have been evaluated for compositional changes associated with diagenesis. It is well known that many Precambrian sedimentary rocks have been affected by potassic and sodic metasomatism (e.g., Nesbitt and Young, 1989; Sutton and Maynard, 1992; Condie, 1993; Fedo et al., 1995, 1997a) and contain cements of varying composition.

Several samples have interstitial carbonate cements or contain detrital carbonate allochems such as pellets and ooids. Since CaO is used in the calculation of Chemical Index of Alteration (CIA, discussed below) values, its presence can skew the results by causing the compositions to shift towards the CN apex of the ternary diagrams (Nesbitt, 2003). Prior to analysis, carbonate-bearing samples (those designated with an R in their sample name) were reacted with dilute 0.1 N HCl at room temperature to remove carbonate. To minimize the effects of Ca-addition, samples that exhibit elevated CaO or Loss on Ignition (LOI) values were discarded in evaluating K-metasomatic effects and assessing paleoweathering conditions.

5.1. K-metasomatism

5.1.1. K-feldspar composition

K-feldspar grains are overwhelmingly dominated by compositions >Or_{95}, with an average of $Or_{96.2}$ (Table 2), which is consistent with a plutonic or metamorphic origin (Trevena and Nash, 1981. However, those grains ≥Or_{90} do not luminesce as would be expected if they originally crystallized at high temperatures; neither do they have compositions typical of authigenic K-feldspar (i.e., >Or_{98}). These grains have an average composition (n = 378 analyses) of SiO_2 64.8%, Al_2O_3 18.6%, K_2O 15.9% (Pure K-feldspar: SiO_2 64.8%, Al_2O_3 18.3%, K_2O 16.9%). Grains analyzed on the microprobe exhibit trace elements (avg. wt. % BaO = 0.23%, SrO = 0.04%, FeO = 0.1%, and MgO = 0.01%, P_2O_5 = 0.03%), which may account for the some of the reduction in K_2O, and the content of Na_2O is typically very low (avg. = 0.4%). The occurrence of subhedral to euhedral grains, the presence of some compositionally pure grains (>Or_{98}) and lack of luminescence suggests that most grains represent original detrital K-feldspars that were partly to completely replaced by authigenic K-feldspar (cf. Fedo et al., 1997a).

5.1.2. Assessing the effects of K-addition

Potassium metasomatism is best evaluated by plotting whole-rock sandstone and mudstone compositions in Al_2O_3–($CaO^* + Na_2O$)–K_2O (A–CN–K) space, where the vertical dimension (% mol Al_2O_3) corresponds with the CIA (Nesbitt and Young, 1984, 1989), and CaO^* represents the Ca in silicate minerals. The A–CN–K plot is useful for evaluating the significance of diagenetic processes resulting in the addition of secondary potassium (Fedo et al., 1995, 1997a,b) and for quantifying the degree of paleoweathering (Nesbitt and Young, 1984; Nesbitt, 2003). A–CN–K relationships can be interpreted in terms of weathering history and paleoclimate (Fedo et al., 1995, 1996, 1997a,b). Johnnie Formation sandstone and mudstone plot in scattered arrays reflecting not only the influences of varied source terranes but also differing degrees of weathering and K-metasomatism (Fig. 8A).

In order to assess the effects of K-metasomatism, an original bulk source composition must be determined so the predicted weathering

Table 2
Electron microprobe data and mineral formulas of plagioclase and alkali feldspar grains (representative analyses). Data for all analyses listed in Schoenborn (2010).

Sample	J1A .1D.2	J1A .1 G.1	J1A .1 M.2	J16A .1D.1	J21A .1A.1	J21A .1B.1	J21A .1 C.1	J45A .1E.1	J45A .1E.2	J66A .1B.1	J66A .1D.1
Unit	2	2	2	2	4	4	4	5	5	6	6
SiO_2	64.76	65.13	64.12	63.73	64.96	64.54	64.52	64.45	64.60	68.49	63.60
TiO_2	bdl	0.01	bdl	bdl	bdl	0.01	0.01	0.01	bdl	0.02	bdl
Al_2O_3	18.65	18.80	18.61	18.38	18.54	18.48	18.36	21.98	22.06	19.89	17.97
FeO	0.03	0.04	0.02	0.06	bdl	0.01	0.03	0.23	0.23	0.08	0.11
MgO	bdl	bdl	bdl	bdl	bdl	bdl	0.01	0.01	bdl	bdl	bdl
MnO	bdl	bdl	bdl	bdl	0.01	bdl	bdl	0.01	0.01	bdl	0.04
CaO	0.04	0.14	bdl	0.03	0.04	0.02	0.05	3.08	3.00	0.48	0.02
Na_2O	0.49	0.58	0.27	0.68	0.35	0.44	0.45	9.96	9.80	11.64	0.15
K_2O	16.17	15.61	16.11	15.36	16.17	15.91	15.78	0.11	0.11	0.08	16.00
P_2O_5	0.03	0.17	bdl	bdl	0.06	0.02	bdl	bdl	0.02	bdl	0.01
BaO	0.25	0.11	0.37	0.29	0.10	0.19	0.15	0.01	0.02	bdl	0.11
SrO	bdl	0.09	0.02	0.05	0.04	0.06	0.08	0.04	0.04	0.02	bdl
Total	100.41	100.67	99.52	98.58	100.25	99.67	99.42	99.88	99.89	100.70	97.99
Si	11.94	11.93	11.940	11.95	11.98	11.97	11.99	11.39	11.40	11.91	12.01
Ti	0.000	0.002	0.000	0.001	0.000	0.001	0.001	0.001	0.000	0.002	0.000
Al	4.054	4.060	4.085	4.063	4.028	4.040	4.021	4.579	4.590	4.075	3.999
Fe	0.004	0.005	0.003	0.009	0.000	0.001	0.004	0.033	0.034	0.012	0.017
Mg	0.001	0.000	0.000	0.000	0.000	0.000	0.002	0.002	0.001	0.000	0.000
Mn	0.000	0.001	0.001	0.001	0.001	0.000	0.000	0.001	0.002	0.000	0.006
Ca	0.008	0.027	0.000	0.006	0.007	0.005	0.009	0.584	0.567	0.090	0.003
Na	0.176	0.205	0.097	0.247	0.125	0.157	0.163	3.414	3.355	3.922	0.053
K	3.804	3.647	3.827	3.674	3.803	3.765	3.741	0.026	0.025	0.018	3.852
P	0.004	0.026	0.000	0.000	0.009	0.002	0.000	0.000	0.003	0.000	0.001
Ba	0.018	0.008	0.027	0.021	0.008	0.014	0.011	0.001	0.001	0.000	0.008
Sr	0.000	0.010	0.002	0.006	0.004	0.006	0.008	0.004	0.004	0.002	0.000
Total	20.01	19.92	19.98	19.98	19.96	19.96	19.95	20.04	19.99	20.03	19.95
	c	c	c	c	c	c	c	c	r	c	c
An	0.00	0.01	0.00	0.16	0.18	0.12	0.24	14.51	14.36	2.23	0.08
Ab	0.04	0.05	0.02	6.28	3.19	4.00	4.16	84.85	85.01	97.33	1.36
Or	0.95	0.94	0.98	93.56	96.64	95.88	95.60	0.64	0.63	0.44	98.56

Sample	J66A .1G.1	J66A .1Q.1	J74A .2C.1	J74A .2E.1	J74A .2E.2	J74A .2F.1	J74A .2F.2	J78A .1A.1	J78A .1A.2	J78A .1B.2	J78A .1B.3	J78A .1C.1	J78A .1E.1
Unit	6	6	7	7	7	7	7	8	8	8	8	8	8
SiO_2	64.27	67.07	64.08	65.47	67.72	67.91	68.02	64.79	64.29	66.41	67.87	67.57	64.31
TiO_2	0.01	0.01	0.02	bdl	bdl	bdl	bdl	0.01	0.02	bdl	bdl	0.01	0.01
Al_2O_3	22.06	19.46	18.64	18.54	19.62	20.28	20.38	18.93	18.93	18.84	19.32	19.38	18.54
FeO	0.03	0.05	bdl	0.02	0.02	0.03	0.03	0.02	0.04	0.05	0.05	0.06	0.05
MgO	bdl	bdl	bdl	bdl	bdl	bdl	bdl	bdl	bdl	0.11	0.01	0.03	bdl
MnO	bdl	0.01	bdl	bdl	bdl	bdl	0.01	bdl	0.01	0.01	bdl	bdl	0.01
CaO	3.22	0.12	0.02	0.02	0.26	0.82	0.79	0.27	0.34	0.31	0.13	0.23	0.02
Na_2O	9.56	10.17	0.24	0.72	9.07	11.39	11.46	1.76	2.27	8.34	11.82	11.75	0.46
K_2O	0.07	2.33	15.84	15.84	3.51	0.08	0.06	13.81	12.86	4.74	0.05	0.08	15.91
P_2O_5	0.01	0.01	0.02	bdl	bdl	0.01	0.01	0.12	0.15	0.03	0.01	0.01	0.02
BaO	bdl	bdl	0.29	0.05	0.02	bdl	bdl	0.09	0.08	0.02	bdl	bdl	0.19
SrO	0.11	0.12	0.03	0.03	0.03	0.06	0.06	0.09	0.05	0.03	0.03	0.01	0.04
Total	99.32	99.34	99.17	100.69	100.24	100.58	100.82	99.88	99.03	98.88	99.28	99.13	99.55
Si	11.40	11.91	11.95	12.00	11.94	11.83	11.82	11.90	11.87	11.95	11.96	11.93	11.95
Ti	0.001	0.001	0.002	0.000	0.000	0.000	0.000	0.001	0.002	0.000	0.000	0.001	0.002
Al	4.612	4.073	4.096	4.006	4.078	4.163	4.175	4.097	4.121	3.996	4.012	4.033	4.061
Fe	0.004	0.008	0.000	0.003	0.003	0.004	0.004	0.004	0.006	0.008	0.007	0.008	0.007
Mg	0.000	0.001	0.000	0.000	0.000	0.000	0.000	0.001	0.001	0.029	0.002	0.008	0.000
Mn	0.000	0.001	0.000	0.000	0.000	0.000	0.001	0.000	0.001	0.001	0.000	0.000	0.002
Ca	0.612	0.022	0.003	0.004	0.049	0.154	0.148	0.054	0.066	0.060	0.024	0.044	0.004
Na	3.287	3.502	0.088	0.254	3.100	3.846	3.862	0.626	0.814	2.910	4.039	4.024	0.167
K	0.015	0.528	3.767	3.705	0.789	0.018	0.012	3.235	3.031	1.087	0.011	0.018	3.770
P	0.001	0.002	0.002	0.000	0.000	0.001	0.001	0.018	0.023	0.005	0.001	0.001	0.002
Ba	0.000	0.000	0.021	0.004	0.002	0.000	0.000	0.007	0.006	0.001	0.000	0.000	0.014
Sr	0.011	0.012	0.003	0.004	0.003	0.006	0.007	0.010	0.006	0.003	0.003	0.001	0.004
Total	19.94	20.06	19.93	19.98	19.96	20.02	20.03	19.95	19.95	20.05	20.06	20.07	19.98
	c	c	c	r	c	c	r	c	r	c	r	c	c
An	15.64	0.55	0.00	0.01	0.00	0.04	0.00	1.38	1.70	1.48	0.60	1.06	0.09
Ab	83.97	86.42	0.03	0.79	0.02	0.96	0.02	15.98	20.81	71.73	99.14	98.49	4.24
Or	0.39	13.02	0.97	0.20	0.98	0.00	0.98	82.64	77.49	26.79	0.26	0.45	95.67

C = core of grain; r = rim of grain; bdl = below detection limit.

path can be derived (Nesbitt and Young, 1989; Fedo et al., 1995). With respect to the Johnnie Formation, data from two units are helpful for identifying bulk source composition. The first group is comprised of Unit 5 mudstone samples with metasomatized CIA values ranging from 67 to 74 (Fig. 8B). A best fit line through the metasomatized values (line 1; r = 0.99) extended back to the feldspar join indicates that the unweathered composition of the Johnnie Formation source had a bulk source plagioclase: K-feldspar ratio of 2:1, nearly identical to that of granodiorite. Unit 2 mudstone samples constitute a second group (Fig. 8C) with metasomatized CIA values between 71 and 73. In

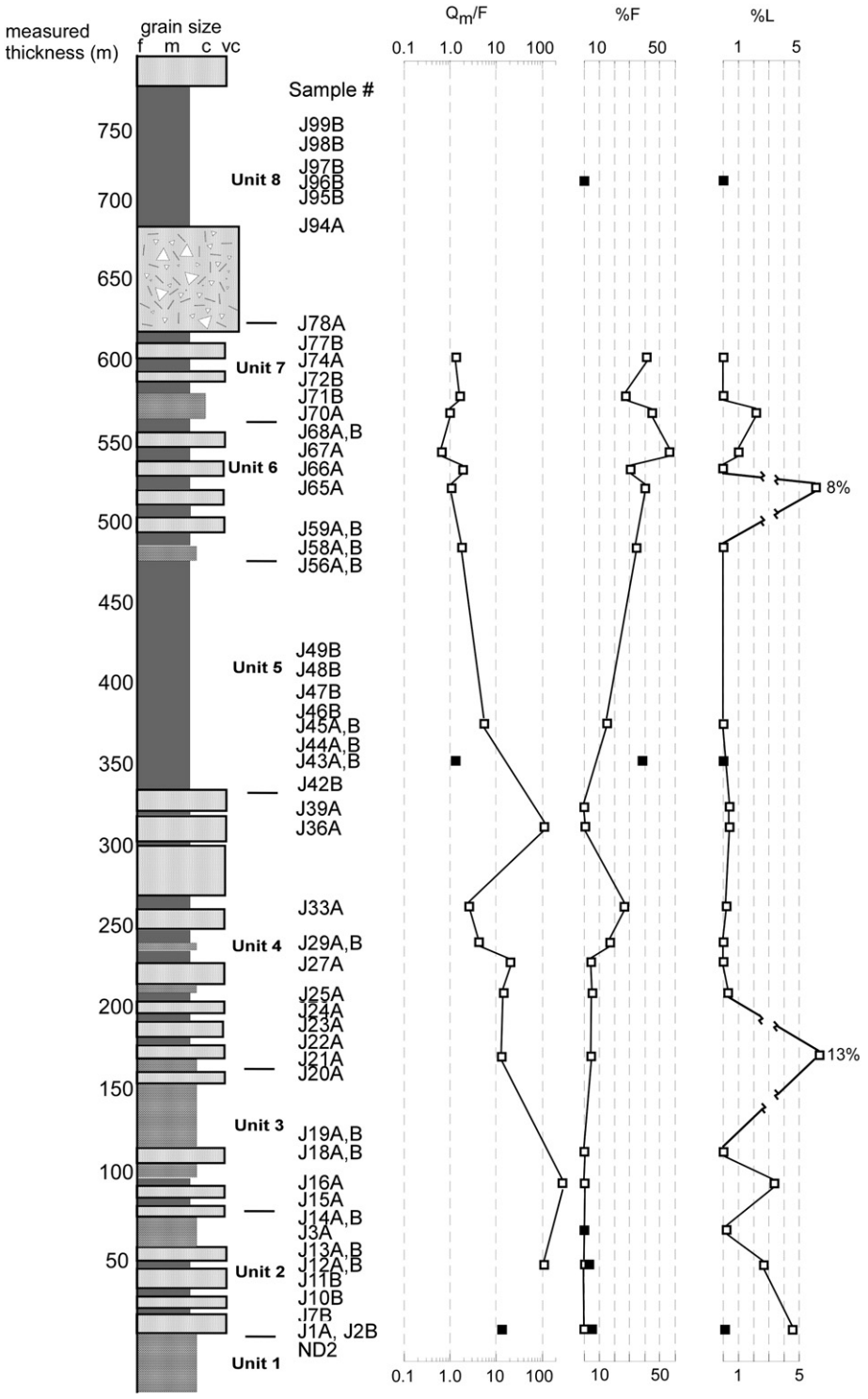

Fig. 3. Schematic stratigraphic section with petrographic parameters for Johnnie Formation sandstone (open squares) and select mudstone (filled squares). Qm = monocrystalline quartz, F = feldspar, L = lithic fragments.

this group, the best-fit straight line (line 1; r = 0.99) passes through Unit 2 sandstone samples, which have feldspar contents close to zero and CIA values that are interpreted to reflect the K-contents of the matrix minerals. Intersection of this regression line with feldspar join suggests the unweathered bulk source composition is very similar to, but slightly more potassic, than that for Unit 5 and a modeled source of ~90% granodiorite and 10% high-K granite derived from geochemical modeling using rare earth elements and selected trace elements (discussed below).

The predicted chemical weathering trend emanating from the plot of the modeled mixture extends upwards from the bulk source composition, roughly parallel to the A–CN boundary (dashed line 2 in Fig. 8B,C) until it intersects the A–K boundary where it turns towards the A apex (Fedo et al., 1995). The samples of Unit 5, however, define a distinct linear trend that departs significantly from the predicted weathering trend, indicating potassium enrichment (most likely illitization of kaolinite), which is graphically defined by a vector (line 3) extending from the weathering trend through the

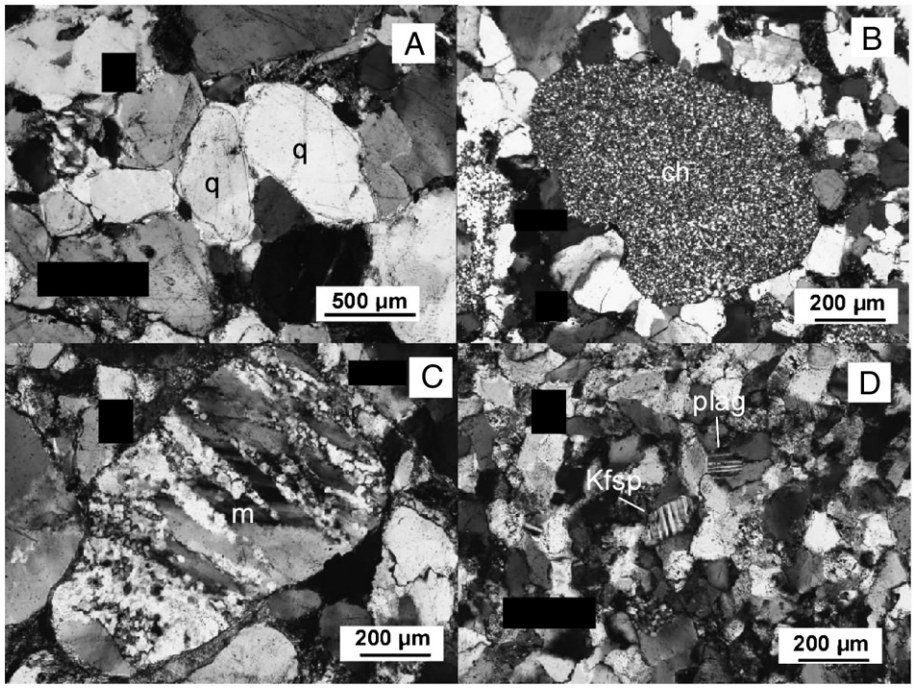

Fig. 4. Photomicrographs of typical lithic fragments in sandstone of the Johnnie Formation in crossed polarized light. (A) Well rounded quartz grains in quartzarenite showing quartz cement overgrowths; (B) Chert rock fragment; (C) Metaquartzite fragment in quartzarenite; and (D) Arkose showing plagioclase and microcline. Abbreviations: q = quartz; ch = chert; m = sheared metaquartzite; plag = plagioclase; Kfsp = microcline.

Table 3
Raw point count data of sandstone and mudstone (representative analyses).

Sample	Unit	Counts	%Qms	%Qmu	%Qp	%Qm	Qm/F	%Q	%F	%L	Grain size
Sandstone											
J1A	2	401	42.4	11.0	25.9	53.4		95.4	0.0	4.6	m
J3A	2	405	37.8	23.2	9.1	61.0		99.6	0.0	0.4	m
J5A	2	402	36.3	13.9	10.4	50.2		99.2	0.0	0.8	m
J9A	2	403	27.8	13.4	2.2	41.2		98.0	0.0	2.0	m
J12A	2	409	44.7	9.5	32.3	54.3	111.0	96.6	0.5	2.7	m
J16A	3	404	51.0	6.9	6.7	57.9	234.0	97.2	0	3.4	m
J17A	3	415	27.7	5.1	3.4	32.8		100	0.0	0	m
J18A	3	403	14.6	2.7	0.5	17.4		100.0	0.0	0.0	m
J21A	4	401	37.9	13.0	28.7	50.9	12.8	82	5	13	m
J25A	4	337	43.6	26.7	13.9	70.3	14.8	94.6	5.0	0.4	f
J27A	4	404	42.8	8.2	1.0	51.0	20.6	95.5	4.5	0.0	f
J29A	4	406	36.5	11.6	7.4	48.0	4.2	83.0	17.0	0.0	f
J33A	4	408	35.8	8.1	3.7	43.9	2.6	73.2	26.4	0.4	f
J36A	4	403	52.6	7.2	17.9	59.8	120.5	98.9	0.5	0.5	c
J39A	4	404	57.7	15.3	12.4	73.0		99.4	0.0	0.6	c
J45A	5	403	15.6	1.2	0.0	16.9	5.7	86.5	13.5	0.0	f
J58A	6	413	43.6	4.1	1.7	47.7	1.8	65.6	34.4	0.0	f
J62A	6	403	38.5	11.7	0	0.50	4.2	80.6	19.0	0.4	f
J65A	6	406	31.0	2.7	6.2	33.7	1.1	51.8	39.9	8.3	f
J66A	6	404	45.3	5.0	6.7	50.2	2.0	69.5	30.5	0.0	f
J67A	6	406	26.8	11.1	4.2	37.9	0.7	42.9	56.1	1.0	f
J70A	7	404	36.9	5.0	6.9	41.8	1.0	53.1	44.7	2.2	f
J71B	7	290	34.5	4.8	23.1	39.3	1.7	72.7	27.3	0.0	f
J74A	7	404	46.3	6.7	2.7	53.0	1.4	58.9	41.1	0.0	f
J78A	8	406	45.3	5.7	7.4	51.0		98.8	0.0	1.3	m
Avg			39.1	9.9	9.6	49.0		83.7	14.6	1.7	
SD			9.3	6.3	8.9	12.6		17.9	17.7	3.0	
Mudstone											
J2B	2	288	33.0	2.8	3.8	35.8	11.4	91.9	7.3	0.1	
J12B	2	373	18.2	2.9	2.9	21.2		98.9	0.0	0.1	
J43B	5	250	30.4	4.4	5.2	34.8	1.4	61.7	38.3	0.0	
J96B	8	406	13.1	1.7	0.5	14.8		100.0	0.0	0.0	
Avg			23.7	3.0	3.1	26.6		88.1	11.4	0.1	
SD			9.6	1.1	2.0	10.3		18.0	18.2	0.1	
Total		10,106									

% = percent of counts; Q = Quartz, F = Feldspar, L = Lithic fragment; m = monocrystalline, p = polycrystalline; s = straight extinction, u = undulatory extinction; $Q_m = Q_{ms} + Q_{mu}$; $Q = Q_m + Q_p$; f = fine, m = medium, c = coarse.

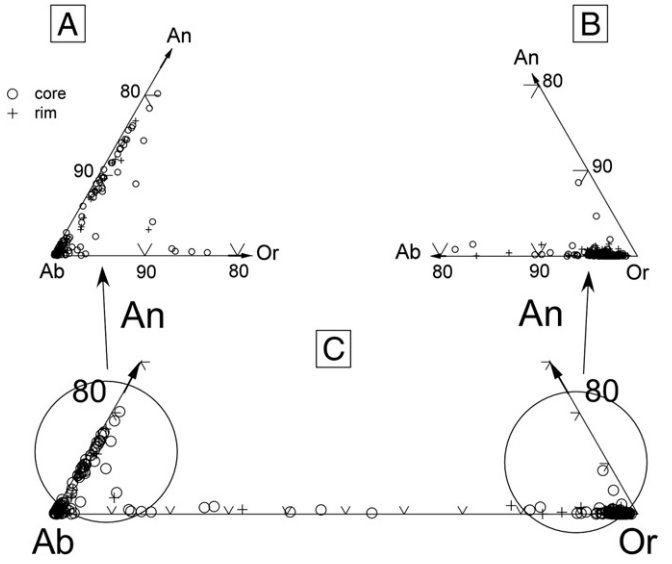

Fig. 5. An–Ab–Or ternary diagram depicting 384 analyses from 240 grains of alkali feldspar and plagioclase from 13 samples of the Johnnie Formation, including 240 cores and 144 rims (crosses). Sixty-two analyses contain more than 90% Ab; (A) Expanded view of the Ab corner. Note that 34 analyses contain more than 96% Ab, which is nearly pure albite; 16 analyses contain more than 99% Ab; such pure compositions indicate an authigenic origin for these grains (Trevena and Nash, 1981); (B) Expanded view of the Or corner. Of the cores, 143 analyses contain more than 90% Or; 145 analyses contain more than 87% Or, which indicates that most grain cores have a high-temperature plutonic or metamorphic origin (Trevena and Nash, 1981). (C) Full Ab–Or join showing all data points.

sample point towards the K-apex. Two Unit 5 sandstone samples (Fig. 8B) that lay outside any predictable composition are populated with albite, likely derived from replacement of other grains (cf. Fedo et al., 1995).

5.2. Na-metasomatism

Plagioclase series evolution is portrayed in (Al_2O_3–K_2O)–CaO*–Na_2O (A–K)–C–N compositional space, where the vertical dimension

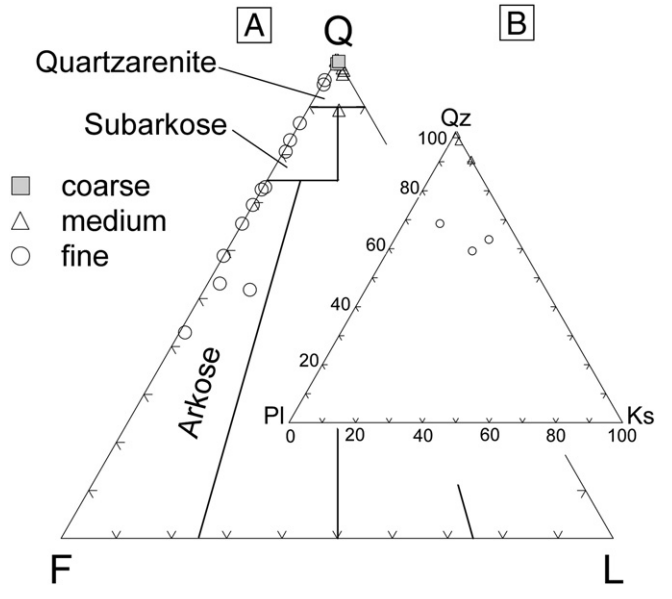

Fig. 6. (A) The sandstone classification QFL diagram of Folk (1974) for sedimentary rocks of the Johnnie Formation, illustrating relationships between composition and grain size. (B) Qz–Pl–Ks diagram of modal compositions of six Johnnie Formation sandstone.

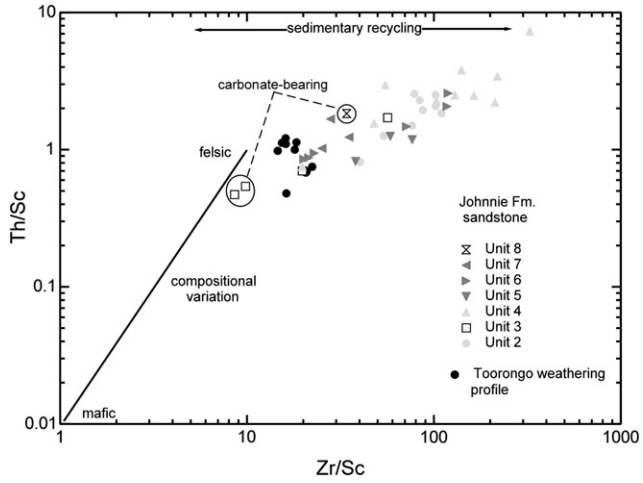

Fig. 7. Plot of Th/Sc versus Zr/Sc for Johnnie Formation sandstone. Enrichment in Zr inferred to be due to efficient sorting and recycling of sediment. In situ (i.e., untransported) soils from the Toorongo weathering profile are shown for comparison, as are samples with Zr concentrations diluted by carbonate minerals.

is the Plagioclase Index of Alteration (PIA; Fig. 9; Fedo et al., 1995). This diagram focuses on the weathering of plagioclase by eliminating the K_2O and Al_2O_3 associated with the making of K-feldspar (Fedo et al., 1995, 1996, 1997a). As with CIA, PIA values for unweathered crystalline bedrocks have values close to 50 and aluminous clay minerals such as kaolinite, illite, and gibbsite plot close to 100.

Sandstone samples from Units 5, 6, and 7 contain plagioclase (Figs. 4D, 9, 10). In (A–K)–C–N compositional space, bulk compositions are mostly sodic, low in calcium, and plot close to, or on the (A–K)–N join in the albite field, consistent with either an albitic source or Na-metasomatism of some plagioclase grains. The PIA values of associated mudstone samples plot near the A–K apex and appear to be depleted in both CaO and Na_2O consistent with intense plagioclase weathering.

Electron microprobe analyses of 39 grains from sample J74A (Unit 7) reveal most grains to be albite (>Ab_{90}), with many displaying high compositional purity (>Ab_{99}); a few are oligoclase (Fig. 10; complete microprobe data set listed in Schoenborn, 2010). All grains are non-luminescent and contain only trace amounts of the elements Sr, Ba and Mn, characteristics that are consistent with overall chemical purity. Of 117 albitic grains examined from the Johnnie Formation, 61% have the nearly pure end member composition typical of authigenic albite; although like K-feldspar, the plagioclases display low trace element contents, and 23% of plagioclase grains exhibit compositions that are not normally considered authigenic (i.e., Ab_{95}–Ab_{97}; Milliken, 1989). Nevertheless, it is concluded that authigenic albite has replaced many detrital plagioclase and K-feldspar grains, similar to those reported by Fedo et al. (1996, 1997a) from the Paleoproterozoic Serpent Formation.

5.3. Paleoweathering

Relative to modeled source bedrock composition (Figs. 11A, B), sandstones and especially mudstones of the Johnnie Formation are depleted in of CaO, Na_2O, Sr, and Ba. CaO is generally depleted up to three orders of magnitude, and Na_2O, is depleted up to two orders of magnitude, whereas Sr, and Ba are depleted up to one order of magnitude relative to the modeled source bedrock composition. These characteristics illustrate the importance of plagioclase weathering in production of the sediments from bedrock.

The “reconstructed” compositions of the mudstones suggest that they underwent moderate to intense weathering conditions. Some mudstone samples that plot on or near the A–K join could have been

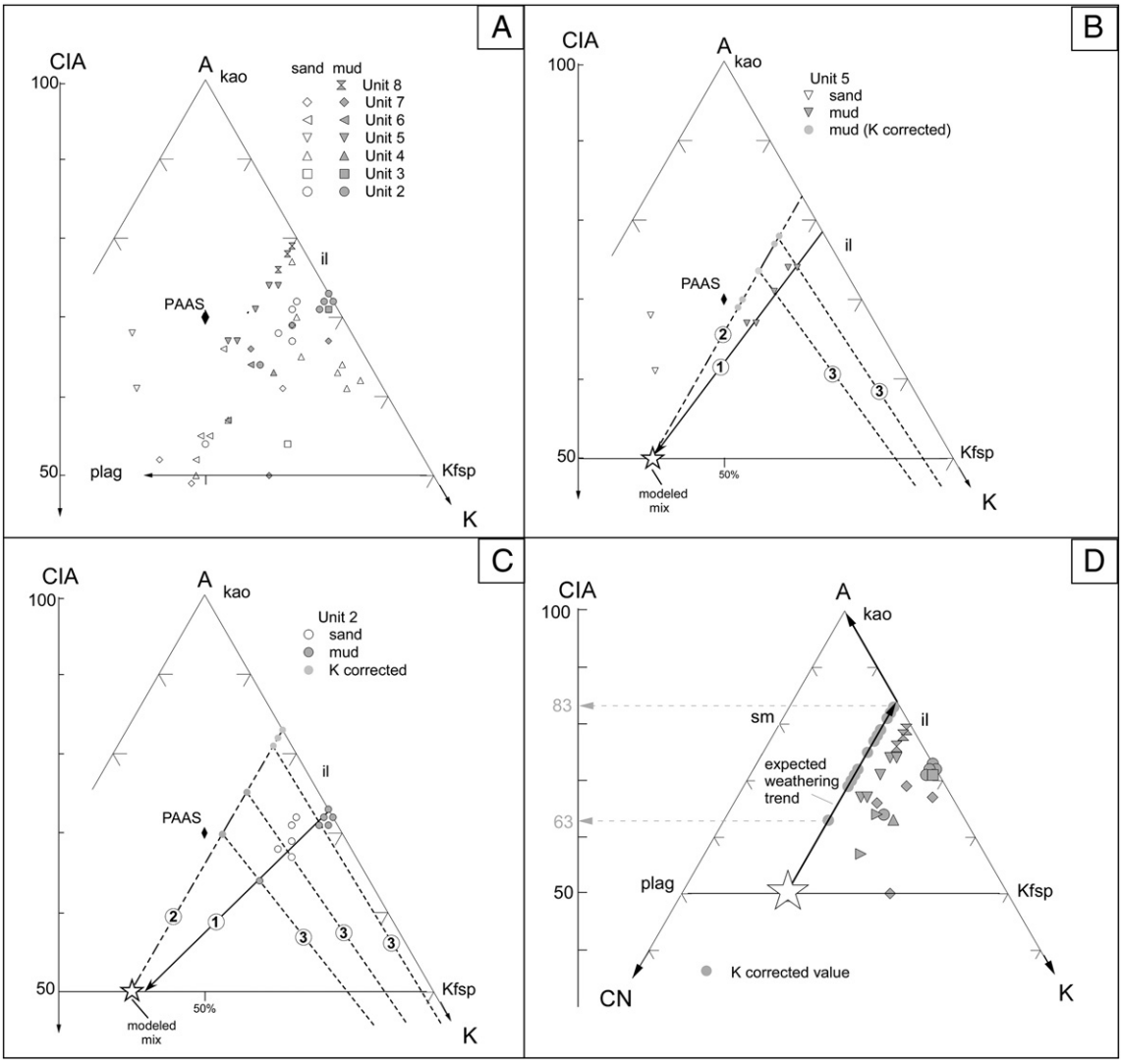

Fig. 8. A–CN–K ternary diagrams for sandstones (open symbols) and mudstones (filled symbols) of the Johnnie Formation. (A) All data. (B) Demonstration of K-metasomatic alteration for Unit 5 mudstones. Solid line is a best-fit straight line through sample points projected back to the feldspar join to indicate bulk rock source composition (line 1). Fine dashed lines (line 2) represent projections used to subtract potassium from illite (Fedo et al., 1995, 1997a). Coarse dashed line represents the predicted weathering trend for the bulk source composition (line 3). Star represents modeled mixture of 90% granodiorite + 10% Hi–K granite and coincides with best-fit line (see text for discussion). (C) Potential weathering and alteration paths for mudstones and sandstones of Unit 2. Solid line (line 1) intersects feldspar join at a point on the feldspar join that suggests a potential bulk source composition for Unit 2 samples that is slightly more potassic than that for mudstones of Unit 5. Fine dashed lines (line 2) represent projections made to subtract potassium from illite (Fedo et al., 1995). Coarse dashed line (line 3) represents the predicted weathering trend for the bulk source composition. (D) Mudstone compositions reconstructed to subtract the effects of K-metasomatism. Note range of CIA values (CIA ≈ 63–83+).

much more highly weathered (different source?) for it is not possible to make a meaningful correction for K-addition when samples fall into this part of the triangle (Figs. 8D, 12). Corrected CIA values of Johnnie Formation mudstone plot in a dispersed linear array (CIA = 63–83) that falls within the range displayed in southern Australia by modern Malacoota River muds and the Lavers Hill weathering profile, both of which experienced moderate weathering in a tectonically stable setting (Duddy, 1980; Nesbitt et al., 1996).

Sandstone samples from the Johnnie Formation display a complete range from mildly to moderately weathered CIA values (corrected CIA = 54–82). Those sandstone and mudstone samples with reconstructed CIA values ≥ 80 could have been supermature, with original CIA values as high as 100, and likely experienced weathering of sufficient intensity and duration to completely remove modal plagioclase and most potassium feldspar from detrital residues (Nesbitt et al., 1997). Considering the chemical data from both mudstones and sandstones, it is concluded that the sediment was predominantly derived from the upper zones (moderate to intensely weathered zones of Nesbitt et al., 1997) of a developed weathering profile. Such soils contain fresh and weathered feldspar as well as aluminous clays produced during chemical weathering.

In A–CN–K compositional space subunits of the Johnnie Formation collectively exhibit a wide range of corrected CIA values (Fig. 8D). The overall compositional diversity exhibited by each subunit is interpreted to reflect temporal changes in the balance between erosion and chemical weathering. Corrected CIA values of sandstone and mudstone samples of Unit 2 plot in distinct clusters (Fig. 8C), possibly suggesting steady state weathering conditions in their source areas (Nesbitt et al., 1997). The abundance of quartz arenite and the paucity of detrital feldspars, particularly plagioclase, in sandstones of the lower Johnnie Formation (Units 2, 3, and 4) suggest intense paleoweathering conditions. In contrast, compositional variability of sandstone and mudstone from the middle to upper Johnnie Formation (Units 4–7) suggests that non-steady state conditions prevailed so that removal of sediment by physical erosion sometimes outpaced geochemical weathering (Nesbitt et al., 1997). Petrographic investigation of sandstone of

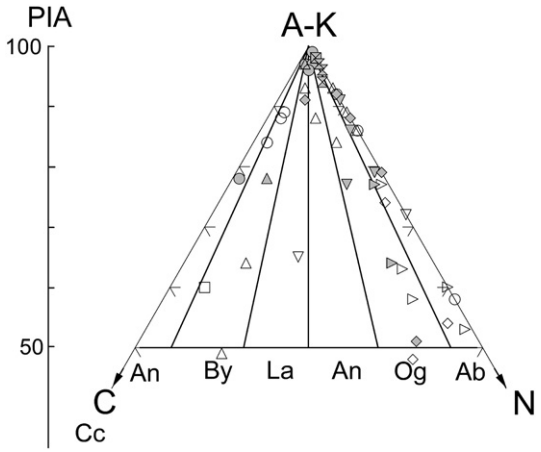

Fig. 9. (A–K)–C–N ternary diagram illustrating whole-rock compositions of Johnnie Formation sands and muds. The A–K vertex corresponds to the plagioclase index of alteration (PIA) which tracks the weathering of the plagioclase series (Fedo et al., 1995). Note that most sandstones from Units 5, 6, and 7 plot in bulk albite or oligoclase compositional space. Unit symbols as in Fig. 7A: An—Anorthite, By—Bytownite, La—Labradorite, Ad—Andesine, Og—Oligoclase, Ab—Albite.

the upper Johnnie Formation (Units 5–7) also reveals variable weathering of feldspar grains. Plagioclase and K-feldspar grains exhibit differing degrees of alteration, ranging from clear to partly vacuolized in plane-polarized light.

6. Provenance

6.1. Petrography

Possible contributors of abundant sand-sized quartz (Fig. 4A) include granitic plutons and recrystallized metamorphic rocks. The abundance of stable rock fragments such as chert (Fig. 4B) and metaquartzite (Fig. 4C) also indicates older sedimentary and metamorphic sources. The optical extinction characteristics of quartz (straight and undulose) as well as the composition of feldspars and plagioclases suggest plutonic or metamorphic sources (Fig. 5; Folk, 1974; Trevena and Nash, 1981). Similarly, stable accessory minerals such as zircon, titanite, tourmaline, apatite, and rutile are all point to felsic-to-intermediate plutonic and metamorphic sources.

6.2. Trace- and rare earth elements

Relative to a modeled source composition (discussed below), sandstones of the Johnnie Formation are depleted in most elements because of quartz dilution. Sandstone compositions also show great swings in magnitude of their concentration due to elemental concentration by specific minerals, such as Zr in zircon (Fig. 11A). Mudstone samples (Fig. 11B) generally show the same overall pattern, but with much less overall range in concentration. An example that illustrates this effect occurs in the change of Zr/Sc between sands and muds, where sands become very depleted in Sc, which preferentially concentrates in the finer grain sizes. Mudstones display modest

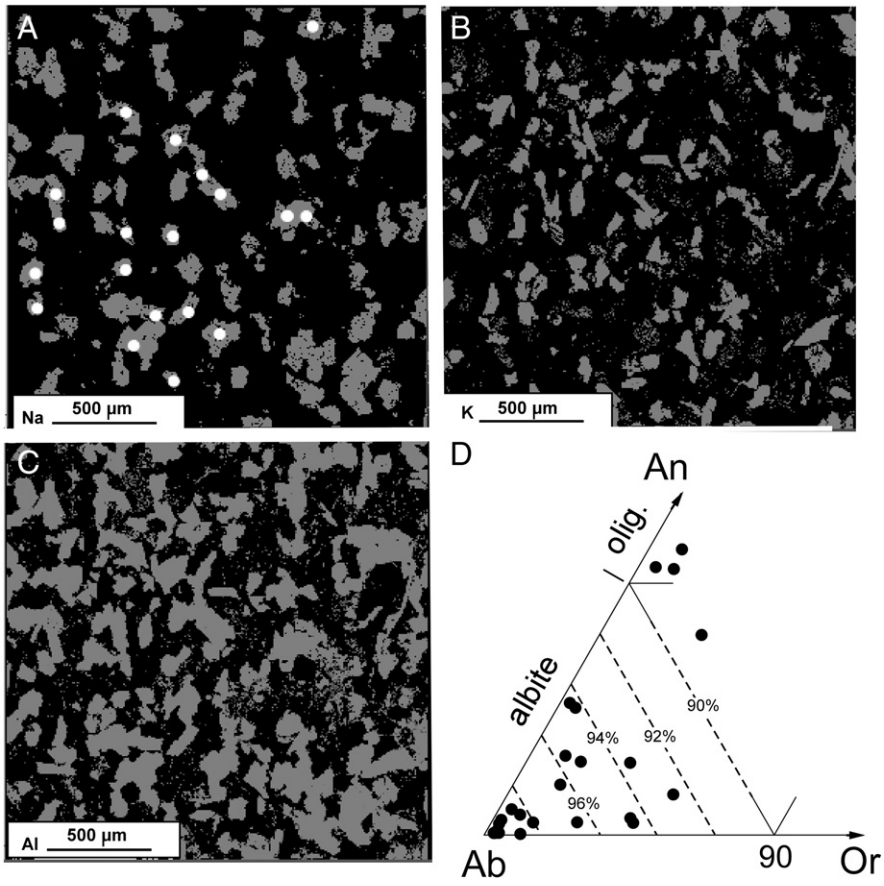

Fig. 10. Electron microprobe element maps from arkose sample J74A (Unit 7) taken 14 m below the unconformity at the base of Unit 8. Grey areas indicate presence of the measured element; black indicates absence. (A) Sodium element map. Grey areas are known from microprobe data to be plagioclase; black area is composed of K-feldspar + quartz. White dots mark grains of plagioclase with microprobe data that are depicted in (D); (B) Potassium element map. Grey areas are known from microprobe data to be K-feldspar; black areas are composed of plagioclase + quartz; (C) Aluminum element map. Grey areas are interpreted as predominantly feldspar (plagioclase + K-feldspar) with minor muscovite; black areas are comprised of quartz. In this sample albitic plagioclase comprises half of total feldspar, and feldspar makes up almost half of total grains. Most plagioclase is pure albite (>Ab99), and is most likely authigenic (Trevena and Nash, 1981); (D) Electron microprobe compositions for plagioclase grains in Or–Ab–An space.

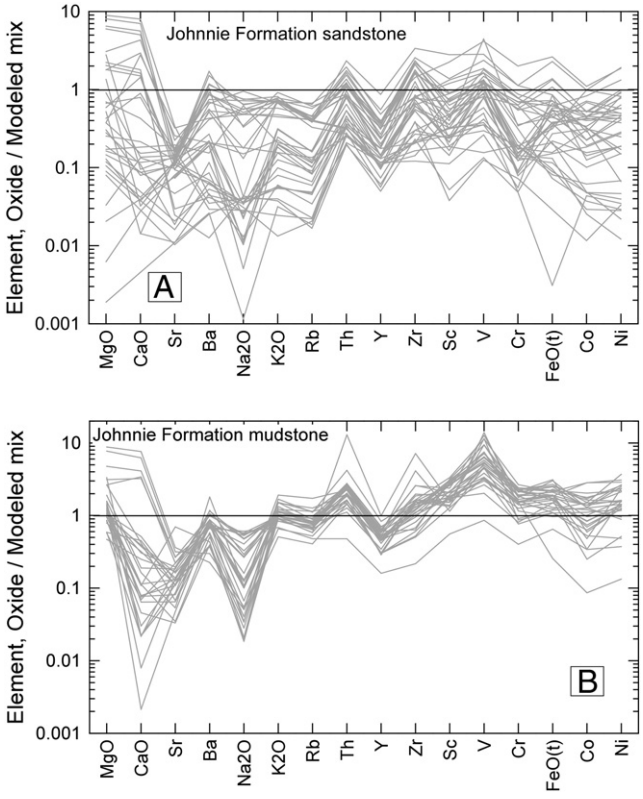

Fig. 11. Oxide and trace element concentrations in (A) sandstones and (B) mudstones of the Johnnie Formation normalized to the modeled mix bulk-source composition. Large ion lithophile elements show a general depletion in CaO and Na_2O relative to the modeled source composition consistent with weathering of plagioclase in the source areas, whereas K_2O, Rb, and Ba in mudstones have normalized values similar to modeled source. Normalization values for V, Cr, Ni, and Co in the modeled mix from average Proterozoic granite in Condie (1993).

enrichment in FeO(t) and the trace elements Th, Zr, Sc, V, Cr, Co, and Ni relative to modeled source bedrock composition, but observed concentrations are not substantial (below a factor of ten). The observed enrichments in Zr, Sc, V, Cr, Co, and Ni in Johnnie Formation mudstone are consistent with the concentration of these elements in accessory minerals in sediment due to sorting.

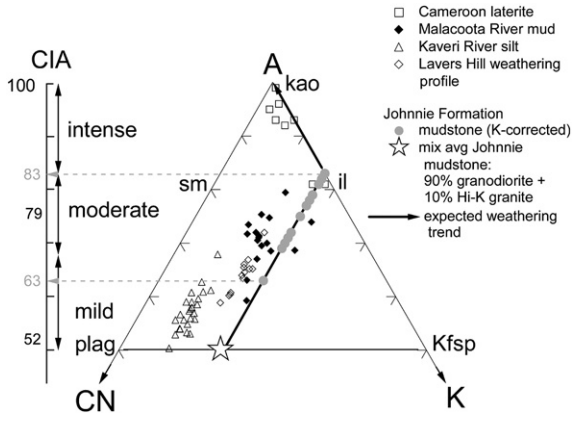

Fig. 12. A–CN–K ternary diagram depicting the similarity between the reconstructed weathering trend for unmetasomatized samples of the Johnnie Formation and modern weathering trends. Double headed arrows illustrate the observed CIA range for sediment weathered under different climatic regimes. The CIA values for Johnnie Formation mudstone (≈63–83) fall within the range associated with mild (CIA≈50–68) to moderate (CIA≈68–81) weathering conditions. Those samples with reconstructed CIA values that plot near the A–K join may have had values associated with intense weathering conditions (CIA≈82–100). Modern profiles: Kaveri River silts, southern India (Singh and Rajamani, 2001); Lavers Hill soil, southeastern Australia (Duddy, 1980); Mallacoota River muds, southeastern Australia (Nesbitt et al., 1996); and Sanaga River laterite soils, East Cameroon (Braun et al., 1997).

Johnnie Formation samples display fairly uniform, chondrite-normalized (CN) REE patterns characteristic of post-Archean sedimentary rocks with $La_{CN}/Yb_{CN} < 15$, $Eu/Eu^* < 0.85$, and $Gd_{CN}/Yb_{CN} = 1.0–2.0$, reflecting the strong influence of quartzofeldspathic source rocks in AUCC and the mixed nature of the source (Fig. 13A, B). Chondrite-normalized REE values for Johnnie Formation sandstone (Fig. 14A) and mudstone (Fig. 14B) show similar patterns strongly suggesting both sediment groups were derived from source regions with similar bulk compositions. For average Johnnie Formation mudstone, the values of $La_{CN}/Sm_{CN} = 4.19 \pm 1.26$, $Gd_{CN}/Yb_{CN} = 1.34 \pm 0.38$, $Eu/Eu^* = 0.63 \pm 0.09$ and $La_{CN}/Yb_{CN} = 9.55 \pm 2.27$, are similar to AUCC ($La_{CN}/Sm_{CN} = 4.18$, $Gd_{CN}/Yb_{CN} = 1.43$, $La_{CN}/Yb_{CN} = 9.44$; $Eu/Eu^* = 0.65$; Taylor and McLennan, 1985) and support a cratonic provenance. Johnnie Formation sediment samples exhibit depletion in Eu, overall LREE fractionation, and depletion in HREE similar to AUCC, reflecting a felsic igneous provenance comprised of granodiorites, monzonites, and granites.

6.3. Detrital zircon ages

Detrital zircon populations vary in age structure through the Johnnie Formation and the Stirling Quartzite and are discussed in

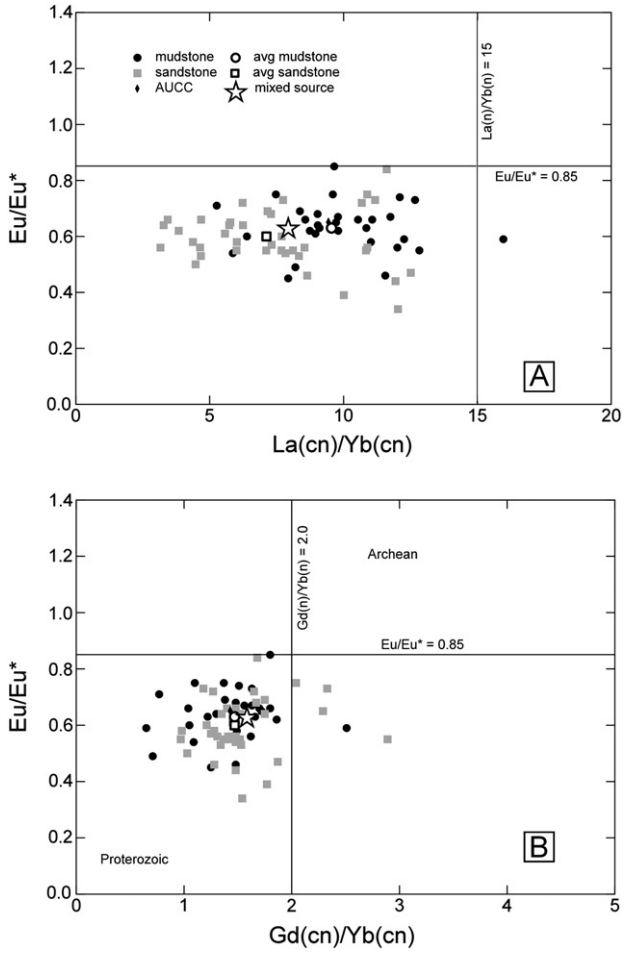

Fig. 13. Plot of Eu/Eu* versus (A) La_{CN}/Yb_{CN} and (B) Gd_{CN}/Yb_{CN} for Johnnie Formation mudstone and sandstone. Johnnie Formation averages and AUCC shown for comparison. Rocks of the Johnnie Formation display fairly uniform REE patterns characteristic of post-Archean sedimentary rocks with $La_{CN}/Yb_{CN} < 15$, $Eu/Eu^* < 0.85$, and $Gd_{CN}/Yb_{CN} = 1.0–2.0$.

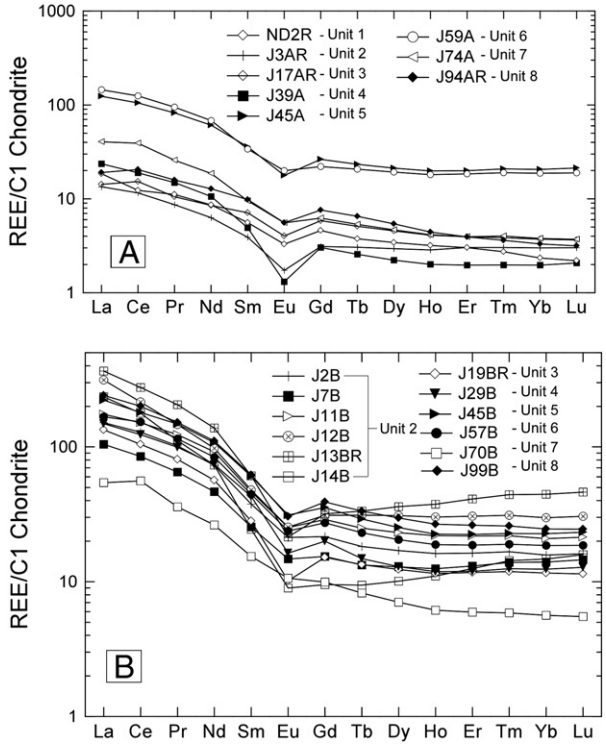

Fig. 14. Chondrite normalized REE distributions for representative sandstones (A) and mudstones (B). Total content of REE in sandstones is low compared to that of mudstones reflecting dilution by quartz. Concentrations normalized to values in C1 chondrite from Anders and Grevesse (1989).

detail elsewhere (Schoenborn et al., in review). Zircon grains in the lower Johnnie Formation (sample J14A) are mostly Paleoproterozoic and Mesoproterozoic (major peak ages: 1749 Ma and 1658 Ma), whereas the middle Johnnie Formation (sample J39A) has a greater proportion of late Grenville age detritus (peak age: 1074 Ma), a significant proportion of older ~1400 Ma Mesoproterozoic grains (peak age: 1428 Ma) and a scattering of Paleoproterozoic and Archean age grains. Paleocurrent directions for Johnnie Formation arenites are generally west–northwest, which indicates that the source area could have been the southwestern region of the Transcontinental Proterozoic province (TPP: Van Schmus et al., 1993). Johnnie Formation detritus is comprised of contributions from diverse sources, including: 1) local bedrock sources located in the rift shoulder, 2) more distal sources in the Laurentian cratonic interior, possibly from as far away as the southern Appalachians, and 3) the Grenville orogen.

6.4. Sediment mixing model

REE and trace element data from a variety of sources were compiled and used to model the relative proportions of end members that contributed sediment to the Johnnie Formation. End members used in mixing calculations (Fig. 15A) were selected from representative granitoid rocks (plutonic rocks and their metamorphic equivalents) in the TPP which have published ages close to the detrital zircon age peaks determined for samples J14A and J39A.

The first end member is a ~1080 Ma granodiorite exposed along the Colorado Front Range (Condie et al., 1995). The second end member is a ~1120 Ma high-potassic granite from the Red Bluff granitic suite characterized by high concentrations of REE (Shannon et al., 1997; Smith et al., 1997). The third end member is comprised of an average of four 1080 Ma diabase intrusions, which are common throughout southeastern California and Arizona (Hammond, 1990; Heaman and Grotzinger, 1992). This provides a wide range of compositions for identifying possible source proportions.

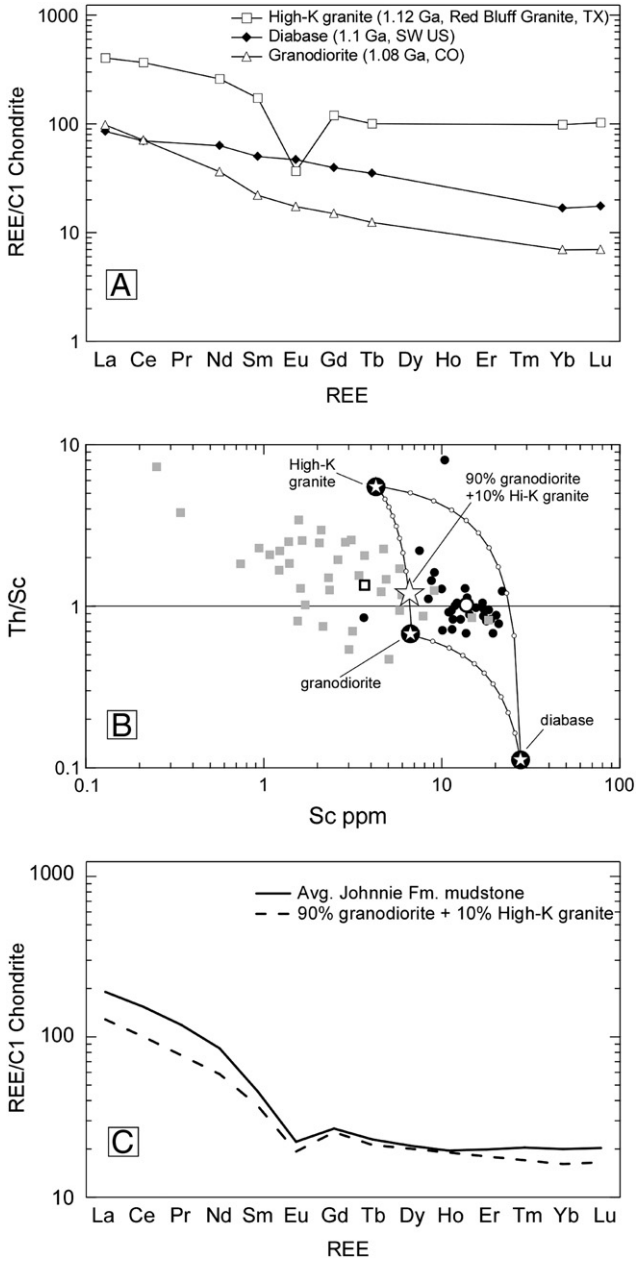

Fig. 15. (A) C1 Chondrite-normalized rare earth element patterns for potential Proterozoic source area end members of Johnnie Formation detritus. Crustal data for the 1.12 Ga high-K granite is sample 711 from the voluminous Stage 2 alkalic granite from the Red Bluff granitic suite, Texas (Shannon et al., 1997); 1.1 Ga diabase is an average of four representative analyses of Middle Proterozoic diabase from the southwestern North America diabase province (Samples IH6, OWL1, EBW1, and RVD1; Hammond, 1990); 1.08 Ga granodiorite is sample CR1-1 from the Front Range, Colorado (Condie et al., 1995). These patterns were mixed in an attempt to reproduce an average source area composition. (B) Th/Sc versus ppm Sc for sandstones and mudstones of the Johnnie Formation. Mixing curves are divided into 10% increments. Note that a mixture of 90% granodiorite + 10% high-K granite balances Th/Sc, whereas granodiorite + diabase does not. A significant contribution from mafic sources is discounted. Average Johnnie Formation mudstone (unfilled dot) and sandstone (unfilled square) shown for comparison. (C) Results from mixing calculations for average Johnnie Formation mudstone.

Using these rock types as potential source contributors, their proportions can be quantitatively modeled (Fig. 15B, C) using a process that conserves mass balance amongst the REEs, and Th/Sc ratio, which are sensitive to bulk source composition (Taylor and McLennan, 1985; Fedo et al., 1997b). A mixture representing 90% granodiorite + 10% high-K granite has an REE content that resembles that of the average of

analyzed mudstones from the Johnnie Formation (Fig. 15B, C; Table 4). Likewise, the Th/Sc ratio of the average mudstone from the Johnnie Formation (Th/Sc = 1.02) is closely replicated by the mixing model (Th/Sc = 1.15). Although the calculated source mixture differs slightly from the average mudstone estimate in LREE, HREE, and the overall fractionation, it has a similar negative Eu anomaly (Eu/Eu* = 0.63). When plotted in A–CN–K compositional space, major elements from mudstones of Unit 5 of the Johnnie Formation form a linear array which, when extended to the feldspar join, yields a plagioclase: K-feldspar ratio of 2:1 (Fig. 8B). The mixture of granodiorite and high-K granite plots in a nearly identical position, and close to that derived from major element data of mudstones of Unit 2. These results reinforce our provenance interpretations.

A ternary mix of 55% granodiorite + 11% high-K granite + 34% diabase also reproduces the Th/Sc ratio of average Johnnie Formation mudstone. The REE pattern produced by this alternative mix is similar to that of our preferred mixing model, but the size of the Eu-anomaly does not match, and compatible trace elements characteristic of mafic rocks (e.g., Cr, Ni, Sc, Co) are all consistent with cratonic shale average composition (Condie, 1993; also see Section 7.2). In addition, the lack of any minerals that could be derived from a mafic provenance would seem to preclude significant detritus from 1.1 Ga diabase. Thus, the mixture of 90% granodiorite and 10% high-K granite provides a better overall chemical fingerprint.

7. Discussion

7.1. Feldspar enrichment in the Johnnie Formation

Understanding the conditions which influenced the composition of the Johnnie Formation is contingent on recognition of the cause of the repetitive stratigraphic occurrence of feldspathic strata in the middle and upper units. The observed increase in detrital feldspar abundance (Fig. 3) has four possible explanations: 1) an increase in tectonism in the source area, which uplifted and exposed feldspar-bearing granites and metamorphic rocks; 2) a change in source area, which brought in new feldspar-bearing detritus; 3) a change in climate, which moderated the rate of chemical weathering through a reduction in either temperature or precipitation; and 4) hydrodynamic sorting, which preferentially segregated comminuted feldspars. Tectonism is discounted because of the absence of lithic arenites with unstable silicic rock fragments—the typical erosional products of topographically rugged areas (Potter, 1978; Franzinelli and Potter, 1983), A change in source area is discounted because the REE patterns from the sedimentary rocks (Figs. 14A, B) are generally similar throughout the entire Johnnie Formation. Although sandstones of Unit 5 have a higher albite content than other units of the Johnnie Formation, their REE patterns display significant Eu-depletion, consistent with derivation from granitic rocks (McLennan, 1989). It is therefore inferred that the sediments of Unit 5 contained significant amounts of K-feldspar at the time of deposition, but the potassic grains were replaced by authigenic albite during diagenesis. A change in paleoweathering conditions might be inferred from a reduction in corrected CIA values from ~82 in mudstones of Unit 2 to ~70–75 for those of Unit 5 (discussed below), but the observed change is quite modest and is not strongly developed in the middle and upper parts of the Johnnie Formation. Consequently, changes in feldspar abundance are attributed to their variable concentration in finer grain sizes as a result of splitting along twinning and cleavage planes (Odom, 1975; Odom et al., 1976; Garzanti, 1986).

7.2. Implications for paleoclimate

It has been long recognized that siliciclastic sedimentary compositions may be linked to prevailing climate (Potter, 1978; Franzinelli and Potter, 1983, Johnsson et al., 1988, 1991; Johnsson, 1993; Nesbitt and Young, 1996). Some modern tropical rivers with low relief watersheds have sands that are quartz arenites (Johnsson et al., 1988, 1991), whereas most rivers draining to the oceans in temperate climate have sands that are subangular lithic arenites (e.g., Potter, 1978). These compositional differences are also highlighted in the geochemistry of suspended-load detritus in modern rivers (McLennan, 1993). First-cycle sands from tropical rivers show a distinctive increase in compositional maturity downstream due to chemical weathering of feldspar and other labile constituents during transport, temporary storage in transient soils, and deposition (Franzinelli and Potter, 1983; Johnsson et al., 1988, 1991). In contrast, comminuted sands derived from glacial systems in an arctic climate are little changed compositionally by transport and sorting by fluvial systems (Nesbitt and Young, 1996). Although variations in feldspar concentration in the Johnnie Formation are linked to grain size, its appearance in middle to upper

Table 4
End member compositions for mixing analysis.

Element	1.12 Ga Red Bluff Granite, #711 (high-K)*		1.1 Ga diabase, SW USA*		1.08 Ga granodiorite*		Avg. Johnnie mudstone		Mix Results* 90% granodiorite + 10% high-K granite*	
	ppm	N	ppm	N	ppm	N	ppm	N	ppm	N
La	94.8	403.9	20.0	85.2	22.9	97.6	44.8	190.7	30.1	128.2
Ce	221.0	366.4	42.0	69.6	42.6	70.6	92.8	153.8	60.4	100.2
Pr							10.6	118.5		
Nd	117.0	258.6	28.5	63.0	16.4	36.3	38.4	84.8	26.5	58.5
Sm	25.4	172.7	7.4	50.1	3.2	22.0	6.7	45.6	5.5	37.1
Eu	2.1	36.8	2.6	46.9	1.0	17.3	1.2	22.2	1.1	19.3
Gd		119.6		39.5		15.0	5.3	26.8		25.4
Tb	3.6	100.3	1.3	35.1	0.5	12.4	0.8	22.9	0.8	21.2
Dy							5.1	20.9		
Ho							1.1	19.5		
Er							3.2	19.9		
Tm							0.5	20.4		
Yb	16.0	98.5	2.7	16.8	1.1	6.9	3.2	20.0	2.6	16.1
Lu	2.5	102.5	0.4	17.5	0.2	7.0	0.5	20.3	0.4	16.5
$(La/Sm)_N$		2.34		1.70		4.43		4.19		3.46
$(Gd/Yb)_N$		1.21		2.36		2.15		1.34		1.58
$(La/Yb)_N$		4.10		5.08		14.03		9.55		7.96
Eu/Eu*		0.26		1.06		0.95		0.63		0.63
Th/Sc		5.58		0.11		0.66		1.02		1.15

N = C1-chondrite normalized value; C1 chondrite values from Anders and Grevesse (1989).
*$Gd_N = (Sm_N \times Tb_N^2)^{1/3}$; $Eu/Eu^* = Eu_N/(Sm_N \times Gd_N)^{1/2}$.

Johnnie Formation sandstone could also have been influenced by changes in weathering intensity, possibly linked to climate.

Regional climate is controlled by latitudinal variations in solar energy that drive atmospheric circulation and the hydrologic cycle. Tropical and temperate latitudes have frequent storms and the highest net precipitation (defined as rainfall minus evaporation), whereas the lowest net precipitation is near the poles and in the subtropics (Berner and Berner, 1987). Although paleogeographic reconstructions for the Late Proterozoic are problematic due to the paucity of paleomagnetic data (Meert and Torsvik, 2004), and complicated by the possibility of true polar wander (Evans, 2003), some reconstructions place Laurentia at near equatorial latitudes during Ediacaran time (McKerrow et al., 1992; Torsvik et al., 1996; Dalziel, 1997; Pisarevsky et al., 2000; Hodych et al., 2004). If our reconstruction is accurate, paleoclimatic conditions during deposition of the Johnnie Formation were likely tropical, characterized by high net precipitation and elevated temperatures.

Climate determines the intensity of weathering by regulating the quantity and composition of water available for reactions (Johnsson, 1993). Humid tropical or subtropical climates are characterized by high precipitation, high average temperature, and efficient production of acidic surface waters, all of which promote intense weathering conditions. Acidic surface waters in warm tropical environments can convert feldspars in sands to clay minerals, and are of sufficient volume to be capable of completely removing all labile phases, thus obliterating the tectonic signal from any residual quartz-rich detritus (Johnsson et al., 1988, 1991). In arid or polar climates, weathering intensity is weak to non-existent because precipitation is either low or locked in ice (Nesbitt, 2003). In these environments physical weathering processes (disaggregation and comminution) predominate over chemical weathering to create detritus with a mineralogy resembling that of the parent bedrock. Few to no new secondary minerals are produced from chemical weathering.

Independent indications of paleolatitude and paleoclimate during Johnnie Formation deposition come from the observation of dolomite, oolite, stromatolites, and cryptalgal laminite preserved in carbonate strata in the stratigraphic section (Fig. 2; Summa, 1993). Most modern carbonate sediments are produced in subtropical to tropical latitudes (0° to 30° N and S; Reading, 1996). In particular, ooids tend to form in warm, shallow, high-energy waters that are carbonate-saturated (Reading, 1996), which is consistent with deposition in a warm, humid paleoclimate.

Corrected Chemical Index of Alteration values (i.e., CIA values that reflect removal of the effects of K-metasomatism) from mudstones of the Johnnie Formation provide an indirect measure of paleoweathering intensity at the time of deposition (Fig. 16). Typically they are much greater than the estimated average shale value of 70 (PAAS; Taylor and McLennan, 1985), indicating relatively more intense weathering conditions. According to the CIA data, weathering intensity varied from moderate to high (corrected values: 72–83) during deposition of mudstones in the lower-to-middle Johnnie Formation (Units 2 to 4), was moderate (corrected values: 63–79) during deposition of the middle-to-upper parts of the formation (Units 6 and 7), then returned to high (corrected values: 79–82) during deposition of the upper Johnnie Formation (Unit 8). These results are consistent with the inferred low paleolatitude for Laurentia and expected paleoclimatic conditions discussed above. Weathering intensity varied from moderate to high during deposition of the lower to middle Johnnie Formation mudstone (Units 2 to 4), scaled back to moderate during deposition of the middle to upper Johnnie Formation (Units 6 and 7), then returned to high during deposition of the upper Johnnie Formation (Unit 8). We interpret these data overall as consistent with a low paleolatitude for Laurentia and warm, humid paleoclimatic conditions during Johnnie deposition.

Evidence for intense weathering conditions during deposition of Johnnie Formation mudstones presented here stands in contrast to other potential evidence of glaciation that may exist in the Rainstorm member, which contains incised valleys of possible glacioeustatic origin (Abolins et al., 2000), and carbonates with strongly negative $\delta^{13}C$ values (Corsetti and Kaufman, 2003). Our data stratigraphically encompass the Johnnie oolite and Rainstorm member units that were removed by incision. Although the Rainstorm member was not directly sampled in this study, none of the mudstone samples, including those collected just below and above the flat-pebble conglomerate, show evidence of true cold weather depositional conditions (i.e., reconstructed CIA values between 50 and 60). Consequently, Johnnie Formation mudstone geochemistry does not record evidence of an extreme paleoclimatic environmental shift in the succession.

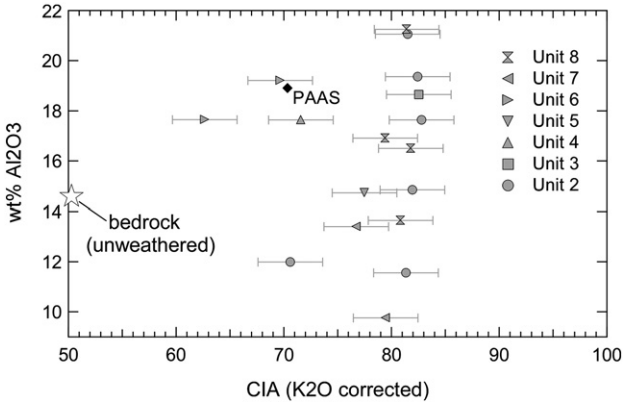

Fig. 16. Al_2O_3 vs. CIA for mudstones of the Johnnie Formation. Bars define the range of natural CIA variation of soil zones of equal weathering intensity, calculated as ±3 units determined from published sediment and soil profile compositional information (Schoenborn, 2010). Samples with bars that overlap are interpreted as possessing feldspars that have experienced equal degrees of weathering—that is, their CIA values are indistinguishable.

7.3. Implications for tectonic setting

Fedo and Cooper (2001) proposed a three-phase tectonic evolution model for the Cordilleran margin in southeastern California: Phase I represents the formation and filling of rift basins; Phase II represents early passive-margin deposition in which local sediment from the rift shoulder mixed with sediment derived from more distal sources; Phase III represents complete covering of cratonic basement by deposition of sediment from the cratonic interior in a mature passive-margin setting. Geochemical characteristics of Johnnie Formation detritus are consistent with derivation from a cratonic source area dominated by a predominantly granitic provenance comprised of old igneous, metamorphic, and sedimentary terranes (i.e., Old Upper Continental Crust of McLennan et al., 1993), a conclusion supported by detrital zircon ages from Johnnie Formation sandstones (Schoenborn, 2010, Schoenborn et al., in review) Uniformity marked by LREE fractionation, flat HREE, and a substantial negative Eu anomaly characterizes the REE patterns of Johnnie Formation strata, indicating their source areas are populated with felsic intrusive rocks formed by intracrustal differentiation (McLennan, 1989; McLennan et al., 1993).

Deposition of the Johnnie Formation likely occurred in a stable tectonic environment characterized by low relief. Johnnie Formation sandstone contains detrital grains that are highly rounded, including quartz, isolated accessory minerals (zircon, titanite, and tourmaline) and durable rock fragments (chert and metaquartzite), indicating that active abrasion was sufficient to eliminate soft rock fragments and to produce some quartz rounding. Feldspars vary from few to abundant in Johnnie formation strata in response to cumulative weathering, mechanical destruction (i.e., time and transport distance), and processes hydraulic sorting in a low-gradient depositional environment (shallow marine shelf).

The stratigraphic architecture of the Johnnie Formation and associated units within the Neoproterozoic stratigraphic succession is one of deposition of facies as regional tabular units that are correlatable across long distances and lap onto the cratonic edge, a setting that is compatible with tectonically quiescent conditions (Fedo and Cooper, 2001). Taken together with depositional environment (distal fluvial-to-shallow marine), uniform thickness, and general lack of rift-related extensional structures during deposition, our geochemical and petrographic data indicate that Johnnie Formation strata were likely deposited as part of a nascent passive-margin succession.

8. Conclusions

Analysis of petrography, feldspar grain composition, and major-, trace-, and rare earth elements of a suite of sandstone and mudstone from the Johnnie Formation yield the following conclusions with regard to the composition of the source area, the weathering conditions that prevailed, and development of the Cordilleran margin in southeastern California:

1) Sandstones of the basal Johnnie Formation are classified as texturally submature quartzarenite with few (<5%) rock fragments (mostly chert and metaquartzite) and scarce potassic feldspar. Variations in grain in roundness suggest the deposit represents a mix of first- and multi-cycle grains. The most common accessory minerals are titanite, zircon, tourmaline, rutile and apatite. Sandstones in the Johnnie Formation become distinctly arkosic up stratigraphic section as reflected in decreasing Q_m/F ratios. They contain both fresh and weathered feldspars. Detrital feldspars, which are concentrated in the finer grained rocks, have been partly to completely replaced by authigenic feldspar. The abundance of highly rounded detrital quartz grains, with less common angular feldspar grains, and the scarcity of durable rock fragments indicates that time and transport distance were sufficient to round quartz, abrade and sort feldspar, and eliminate soft rock fragments. These textural characteristics, when combined with existing data on stratigraphic architecture, are consistent with quiescent tectonic conditions characterized by low relief, and deposition of Johnnie Formation strata in a passive-margin setting.
2) In A–CN–K compositional space, sandstones and mudstones of the Johnnie Formation depart from the expected weathering trend and show evidence of modest K-metasomatism. Sandstones in the middle-to-upper parts of the Johnnie Formation were subjected to sodium metasomatism, as shown by the presence of authigenic plagioclase grains of high compositional purity ($>Ab_{99}$). Corrected CIA values for mudstones of the Johnnie Formation (range: 63 to 83; those samples ≥80 could have had original values as high as 100) suggest that these sediments were generated under moderate to potentially very intense paleoweathering conditions. Slight variations in paleoweathering of Johnnie Formation mudstones from moderate intensity to high intensity are interpreted as consistent with a low paleolatitude and deposition of Johnnie Formation strata under constant warm, humid paleoclimatic conditions.
3) Concentration of the incompatible trace elements Ba, Zr and Th in mudstones of the Johnnie Formation resembles those of a modeled source mix, which is felsic in composition. Relative to C1-chondrite, the general pattern REE representing average Johnnie Formation mudstone is characterized by LREE fractionation (average $La_{CN}/Sm_{CN} = 4.19$), relatively flat HREE (average $Gd_{CN}/Yb_{CN} = 1.34$), and a negative Eu anomaly (average $Eu/Eu^* = 0.63$). Johnnie Formation samples show almost no fractionation of REEs in sandstones relative to mudstones, suggesting that both sediment groups were derived from source regions with similar bulk compositions. Average values of Eu/Eu*, Th/Sc, and Th/U in Johnnie Formation mudstone are characteristic of cratonic source areas populated with felsic intrusive rocks.
4) The REE pattern and Th/Sc ratio of average Johnnie Formation mudstone are closely replicated by mixing Proterozoic source rocks exposed in the Trancontinental Proterozoic province in the following proportions: 90% granodiorite + 10% high-K granite, which suggests that granitic sources were major contributors to Johnnie Formation sediment. This precludes significant contributions from diabase, which is also consistent with petrographic and other geochemical observations. Taken together with known paleocurrent directions and detrital zircon ages, geochemistry and source modeling results suggest Johnnie Formation sediment could have been derived from source areas in the southwestern region of the Transcontinental Proterozoic province.

Acknowledgements

This research was supported by the National Science Foundation (NSF) grant EAR-99-09308 to CMF. We thank Balz Kamber of the University of Queensland, Australia (now of Laurentian University, Canada) for collecting the major- and trace-element geochemical data, Joe Wooden of the U.S. Geological Survey SHRIMP-RG lab at Stanford University for help in collecting the detrital zircon U–Pb isotopic data, and Harvey Belkin of the USGS in Reston, Virginia for help in collecting the electron microprobe data. We thank Grant Young, John Hanchar, David Lambert, and Mark Reeves for commenting on early versions of the manuscript. We also thank the journal referees for helping us clarify a number of points and improving several aspects of this paper.

References

Abolins, M., Oskin, R., Prave, A.R., Summa, C.L., Corsetti, F.A., 2000. Neoproterozoic glacial record in the Death Valley region, California and Nevada. In: Lageson, D.R.P., Stephen, G., Lahren, M.M. (Eds.), Geol. Soc. Amer., Boulder. Geological Society of America Field Guide 2, Great Basin and Sierra Nevada, pp. 319–335.
Anders, E., Grevesse, N., 1989. Abundances of the elements: meteoritic and solar. Geochim. Cosmochim. Acta 53, 197–214.
Berner, E.K., Berner, R.A., 1987. The Global Water Cycle. Prentice Hall, Inc. 397p.
Bond, G.C., Christie-Blick, N., Kominz, M.A., Devlin, W.J., 1985. An early Cambrian rift to post-rift transition in the Cordillera of western North America. Nature 315, 742–745.
Borg, S.G., DePaolo, D.J., 1994. Laurentia, Australia and Antarctica as a Late Proterozoic supercontinent: constraints from isotopic mapping. Geology 22, 307–310.
Braun, J.-J., Viers, J., Dupre, B., Polve, M., Ndam, J., Muller, J.-P., 1997. Solid/liquid REE fractionation in the lateritic system of Goyoum, East Cameroon: the implication for the present dynamics of the soil covers of the humid tropical regions. Geochim. Cosmochim. Acta 62, 273–299.
Buchan, K.L., Ernst, R.E., Hamilton, M.A., Mertanen, S., Pesonen, L.J., Elming, S.-A., 2001. Rodinia: the evidence from integrated paleomagnetism and U–Pb geochronology. Precambrian Res. 110, 9–32.
Cawood, P.A., Pisarevsky, S.A., 2006. Was Baltica right-way-up or upside-down in the Neoproterozoic? J. Geol. Soc. London 163, 753–759.
Clapham, M.E., Corsetti, F.E., 2005. Deep valley incision in the terminal Neoproterozoic (Ediacaran) Johnnie Formation, eastern California, USA: tectonically or glacially driven? Precambrian Res. 141, 154–164.
Condie, K.C., 1993. Chemical composition and evolution of the upper continental crust: contrasting results from surface samples and shales. Chem. Geol. 104, 1–37.
Condie, K.C., Dengate, J., Cullers, R.L., 1995. Behavior of rare earth elements in a paleoweathering profile on granodiorite in the Front Range, Colorado. Geochim. Cosmochim. Acta 59, 279–294.
Corsetti, F.A., Kaufman, A.J., 2003. Stratigraphic investigations of carbon isotope anomalies and Neoproterozoic ice ages in Death Valley, California. Geol. Soc. Amer. Bull. 115, 916–932.
Crowell, J.C., 1999. Pre-Mesozoic Ice Ages: their bearing on understanding the climate system. Geol. Soc. Am. Mem. 192, 106p.
Dalziel, I.W.D., 1991. Pacific margins of Laurentia and East–Antarctica–Australia as a conjugate rift pair: evidence and implications for an Eocambrian supercontinent. Geology 19, 598–601.
Dalziel, I.W.D., 1997. Neoproterozoic–Paleozoic geography and tectonics: review, hypothesis, environmental speculation. Geol. Soc. Am. Bull. 109, 16–42.
Duddy, I.R., 1980. Redistribution and fractionation of rare-earth and other elements in a weathering profile. Chem. Geol. 30, 363–381.
Evans, D.A., 2003. True polar wandering and supercontinents. Tectonophysics 362, 303–320.

Eyles, N., Janusczcak, N., 2004. 'Zipper rift': a tectonic model for Neoproterozoic glaciations during the breakup of Rodinia after 750 Ma. Earth Sci. Rev. 65, 1–73.
Fedo, C.M., Eriksson, K.A., Krogstad, E.J., 1996. Geochemistry of shales from the Archean (~3.0 Ga) Buhwa Greenstone Belt, Zimbabwe: implications for provenance and source-area weathering. Geochim. Cosmochim. Acta 60, 1751–1763.
Fedo, C.M., Nesbitt, H.W., Young, G.M., 1995. Unraveling the effects of potassium metasomatism in sedimentary rocks and paleosols, with implications for paleoweathering conditions and provenance. Geology 23, 921–924.
Fedo, C.M., Young, G.M., Nesbitt, H.W., Hanchar, J.M., 1997a. Potassic and sodic metasomatism in the Southern Province of the Canadian Shield: evidence from the Paleoproterozoic Serpent Formation, Huronian Supergroup. Canada. Precambrian Res. 84, 17–36.
Fedo, C.M., Young, G.M., Nesbitt, H.W., 1997b. Paleoclimatic control on the composition of the Paleoproterozoic Serpent Formation, Huronian Supergroup, Canada: a greenhouse to icehouse transition. Precambrian Res. 86, 201–223.
Fedo, C.M., Cooper, J.D., 2001. Sedimentology and sequence stratigraphy of Neoproterozoic and Cambrian units across a craton-margin hinge zone, southeastern California, and implications for the early evolution of the Cordilleran margin. Sediment. Geol. 141–142, 501–522.
Ferri, F., Rees, C., Nelson, J., Legun, A., 1999. Geology and mineral deposits of the northern Kechika Trough, between Gataga River and the 60th parallel. BC Min. Energy and Mines Bull. 107, 122.
Folk, R.L., 1974. Petrology of Sedimentary Rocks. Hemphill Publishing Company. 182p.
Franzinelli, E., Potter, P.E., 1983. Petrology, chemistry and texture of modern river sands, Amazon River system. J. Geol. 91, 23–39.
Garzanti, E., 1986. Source rock versus sedimentary control on the mineralogy of deltaic volcanic arenites (Upper Triassic, northern Italy). J. Sediment. Petrol 56, 267–275.
Hammond, J.G., 1990. Middle Proterozoic diabase intrusions in the southwestern U.S.A. as indicators of limited extensional tectonism. In: Gower, C.F., Rivers, T., Ryan, A.B. (Eds.), Mid-Proterozoic Laurentia-Baltica: Geol. Assoc. Can. Spec. Pap., 38, pp. 517–531.
Heaman, L.M., Grotzinger, J.P., 1992. 1.08 Ga diabase sills in the Pahrump Group, California: implications for development of the Cordilleran miogeocline. Geology 20, 637–640.
Hodych, J.P., Cox, R.A., Kosler, J., 2004. An equatorial Laurentia at 550 Ma confirmed by Grenvillian inherited zircons dated by LAM ICP-MS in the Skinner Cove volcanics of western Newfoundland: implications for inertial interchange true polar wander. Precambrian Res. 129, 93–113.
Hoffman, P.F., Kaufman, A.J., Halverson, G.P., Schrag, D.P., 1998. A Neoproterozoic snowball Earth. Science 281, 1342–1346.
Hoffman, K.H., Schrag, D.P., 2002. The snowball earth hypothesis: testing the limits of global change. Terra Nova 14, 129–155.
Hurowitz, J.A., McLennan, S.M., 2005. Geochemistry of Cambro-Ordovician sedimentary rocks of the northeastern United States: changes in sediment sources at the onset of Taconian orogenesis. Geology 113, 571–587.
Johnsson, M.J., 1993. The system controlling the composition of clastic sediments. In: Johnsson, M.J., Basu, A. (Eds.), Processes Controlling the Composition of Clastic Sediments: Geol. Soc. Amer. Spec. Pap., 284, pp. 1–19.
Johnsson, M.J., Stallard, R.F., Lundberg, N., 1991. Controls on the composition of fluvial sands from a tropical weathering environment: sands of the Orinoco River drainage basin, Venezuela and Columbia. Geol. Soc. Am. Bull. 103, 1622–1647.
Johnsson, M.J., Stallard, R.F., Meade, R.H., 1988. First-cycle quartz arenites in the Orinoco River basin, Venezuela and Columbia. J. Geol. 96, 103–227.
Karlstrom, K.E., Ahall, K.-I., Harlan, S.S., Williams, M.L., McLelland, J., Geissman, J.W., 2001. Long-lived (1.8–1.0 Ga) convergent orogen in southern Laurentia, its extensions to Australia and Baltica, and implications for refining Rodinia. Precambrian Res 111, 5–30.
Kaufman, A.J., Jacobsen, S.B., Knoll, A.H., 1993. The Vendian record of Sr and C isotopic variations in seawater: implications for tectonics and paleoclimate. Earth Planet. Sci. Lett. 120, 409–430.
Kaufman, A.J., Knoll, A.H., Awramik, S.M., 1992. Biostratigraphic and chemostratigraphic correlation of Neoproterozoic sedimentary successions: Upper Tindir Group, northwestern Canada, as a test case. Geology 29, 181–185.
Kaufman, A.J., Knoll, A.H., Narbonne, G.M., 1997. Isotopes, ice ages, and terminal Proterozoic earth history. Proc. Nat. Acad. Sci. 94, 6600–6605.
Levy, M., Christie-Blick, N., 1991. Tectonic subsidence of the early Paleozoic passive continental margin in eastern California and southern California. Geol. Soc. Am. Bull. 103, 1590–1606.
Li, Z.X., Bogdanova, S.V., Collins, A.S., Davidson, A., DeWaele, B., Ernst, R.E., Fitzsimons, I.C.W., Fuck, R.A., Gladkochub, D.P., Jacobs, J., Karlstrom, K.E., Lu, S., Natapov, L.M., Pease, V., Pisarevsky, S.A., Thrane, K., Verikovsky, V., 2008. Assembly, configuration, and break-up history of Rodinia: a synthesis. Precambrian Res. 160, 179–210.
Link, P.K., Christie-Blick, N., Devlin, W.J., Easton, D.P., Horodyski, R.J., Levy, M., Miller, J.M.G., Pearson, R.C., Prave, A., Stewart, J.H., Winston, D., Wright, L.A., Wrucke, C.T., 1993. In: Reed Jr., J.C., Bickford, M.E., Houston, R.S., Link, P.K., Rankin, D.W., Sims, P.K., Van Schmus, W.R. (Eds.), Geol. Soc. Amer., C-2. Precambrian: Conterminous U.S, The Geology of North America, pp. 463–595.
McKerrow, W.S., Scotese, C.R., Brasier, M.D., 1992. Early Cambrian continental reconstructions. J. Geol. Soc. London 149, 599–606.
McLennan, S.M., 1989. Rare earth elements in sedimentary rocks: influence of provenance and sedimentary processes. Mineralogical Soc. Amer., Rev. Mineralogy 21, 169–200.
McLennan, S.M., 1993. Weathering and global denudation. J. Geol. 101, 295–303.
McLennan, S.M., Hemming, S., McDaniel, D.K., Hanson, G.N., 1993. Geochemical approaches to sedimentation, provenance, and tectonics. In: Johnson, M.J., Basu, A. (Eds.), Processes Controlling the Composition of Clastic Sediments: Boulder, Colorado: Geol. Soc. Amer. Sp. Pap., 284, pp. 21–40.
Meert, J.G., Torsvik, T.H., 2004. Paleomagnetic constraints on Neoproterozoic 'Snowball Earth' continental reconstructions. In: Jenkins, G.S., McMenamin, M.A.S., McKay, C.P., Sohl, L. (Eds.), The extreme Proterozoic: geology, geochemistry, and climate. American Geophysical Union. AGU Monograph 146, Washington, D.C, pp. 5–11.
Mehring, J.L., McBride, E.F., 2007. Origin of modern quartzarenite beach sands in a temperate climate, Florida and Alabama. U.S.A. Sediment. Geol. 201, 432–445.
Miller, J.M.G., 1985. Glacial and syntectonic sedimentation: the upper Proterozoic Kingston Peak Formation, southern Panamint Range, eastern California. Geol. Soc. Am. Bull. 96, 1537–1553.
Miller, J.M.G., 1986. Upper Proterozoic glaciogenic rift-valley sedimentation: Upper Mount Rodgers Formation, southwestern Virginia. Am. Assoc. Petrol. Geol. Bull. 70, 621.
Milliken, K.L., 1989. Petrography and composition of authigenic feldspars, Oligocene Frio Formation, south Texas. J. Sediment. Petrol. 59, 361–374.
Moores, E.M., 1991. Southwest U.S.–East Antarctic (SWEAT) connection: a hypothesis. Geology 19, 425–428.
Nesbitt, H.W., 2003. Petrogenesis of siliciclastic sediment and sedimentary rocks. In: Lentz, D.R. (Ed.), Geochemistry of Sediment and Sedimentary Rocks. Geol. Assoc. Evolutionary Considerations to Mineral-Deposit-Forming Environments, Geotext4, Canada, pp. 39–51.
Nesbitt, H.W., Fedo, C.M., Young, G.M., 1997. Quartz and feldspar stability, steady and non-steady-state weathering, and petrogenesis of siliciclastic sands and muds. J. Geol. 105, 173–191.
Nesbitt, H.W., Markovics, G., 1997. Weathering of the Toorongo Granodiorite, storage of elements in weathering profiles, and genesis of siliciclastic sediment. Geochim. Cosmochim. Acta 61, 1653–1670.
Nesbitt, H.W., Young, G.M., 1984. Prediction of some weathering trends of plutonic and volcanic rocks based on thermodynamic and kinetic considerations. Geochim. Cosmochim. Acta 48, 1523–1534.
Nesbitt, H.W., Young, G.M., 1989. Formation and diagenesis of weathering profiles. J. Geol. 97, 129–147.
Nesbitt, H.W., Young, G.M., 1996. Petrogenesis of sediment in the absence of chemical weathering: effects of abrasion and sorting on bulk composition and mineralogy. Sedimentology 43, 341–358.
Nesbitt, H.W., Young, G.M., McLennan, S.M., Keays, R.R., 1996. Effects of chemical weathering and sorting on the petrogenesis of siliciclastic sediment, with implications for provenance studies. J. Geol. 104, 525–542.
Odom, I.E., 1975. Feldspar–grain size relations in Cambrian arenites, upper Mississippi Valley. Jour. Sediment Pet. 45, 636–650.
Odom, I.E., Doe, T.W., Dott, R.H., 1976. Nature of feldspar-grain size relations in some quartz-rich sandstone. J. Sediment. Petrol. 46, 862–870.
Pisarevsky, S.A., Komissarova, R.A., Khramov, A.N., 2000. New paleomagnetic result from Vendian red sediments in Cisbaikalia and the problem of the relationship of Siberia and Laurentia in the Vendian. Geophys. J. Int. 140, 598–610.
Potter, P.E., 1978. Petrology and chemistry of modern big river sands. J. Geol. 86, 423–449.
Prave, A.R., 1999. Two diamictites, two cap carbonates, two $\delta^{13}C$ excursions, two rifts: the Neoproterozoic Kingston Peak Formation, Death Valley, California. Geology 27, 339–342.
Reading, H.G., 1996. Sedimentary Environments: Processes, Facies, and Stratigraphy. Blackwell Science Ltd., London. 688p.
Schoenborn, W. A., 2010. Geochemistry of the Neoproterozoic Johnnie Formation and Stirling Quartzite, southern Nopah Range, California: deciphering the roles of climate, tectonics, and sedimentary process in reconstructing the early evolution of a rifted continental margin. Unpub. Ph.D. Dissertation, George Washington University.
Schoenborn, W.A., Fedo, C.M., and Farmer G.L., 2011. Provenance of the Neoproterozoic Johnnie Formation, southeastern California, determined by detrital zircon geochronology and Nd isotope geochemistry. Precambrian Research (in review).
Shannon, W.M., Barnes, C.G., Bickford, M.E., 1997. Grenville magmatism in west Texas: petrology and geochemistry of the Red Bluff Granite suite. J. Pet. 38, 1279–1305.
Singh, P., Rajamani, V., 2001. Geochemistry of the floodplain sediment of the Kaveri River, southern India. J. Sediment. Res. 71, 50–60.
Smith, D.R., Barnes, C., Shannon, W., Roback, R., James, E., 1997. Petrogenesis of Mid-Proterozoic granitic magmas: examples from central and west Texas. Precambrian Res. 85, 53–79.
Sohl, L.E., Christie-Blick, N., Kent, D.V., 1999. Paleomagnetic polarity reversals in Marinoan (ca. 600 Ma) glacial deposits of Australia: implications for the duration of low-latitude glaciation in Neoproterozoic time. Bull. Geol. Soc. Amer. 111, 1120–1139.
Stewart, J.H., 1970. Upper Precambrian and Lower Cambrian strata in the southern Great Basin California and Nevada. U.S. Geol. Surv. Prof. Paper 620.
Stewart, J.H., 1972. Initial deposits of the Cordilleran geosyncline: evidence of a Late Precambrian (<850 m.y.) continental separation. Geol. Soc. Am. Bull. 83, 1345–1360.
Summa, C.L., 1993. Sedimentologic, stratigraphic, and tectonic controls of a mixed carbonate-siliciclastic succession: Neoproterozoic Johnnie Formation, southeast California. Unpub. Ph.D. Dissertation, Massachusetts Institute of Technology.
Sutton, S.J., Maynard, J.B., 1992. Multiple alteration events in the history of a sub-Huronian regolith at Lauzon Bay, Ontario. Can. J. Earth Sci. 30, 1209–1223.
Taylor, S.R., McLennan, S.M., 1985. The Continental Crust: its Composition and Evolution Geoscience Texts. Blackwell Scientific Publications. 312p.
Torsvik, T.H., Smethurst, M.A., Meert, J.G., Van der Voo, R., McKerrow, W.S., Sturt, B.A., Brasier, M.D., Walderhaug, H.J., 1996. Continental breakup and collision in the Neoproterozoic and Paleozoic—a tale of Baltica and Laurentia. Earth Sci. Rev. 40, 229–258.
Trevena, A.S., Nash, W.P., 1981. An electron microprobe study of detrital feldspar. J. Sediment. Petrol. 51, 137–150.
Van Schmus, W.R., Bickford, M.E., Anderson, J.L., Bender, E.E., Anderson, R.R., Bauer, P.W., Robertson, J.M., Bowring, S.A., Condie, K.C., Denison, R.E., Gilbert, M.C., Grambling, J.A., Mawer, C.K., Shearer, C.K., Hinze, W.J., Karlstrom, K.E., Kisvarsanyi, E.B., Lidiak, E.G., Reed

Jr., J.C., Sims, P.K., Tweto, O., Silver, L.T., Treves, S.B., Willims, M.L., Wooden, J.L., 1993. Transcontinental Proterozoic provinces. In: Reed Jr., J.C., Bickford, M.E., Houston, R.S., Link, P.K., Rankin, D.W., Sims, P.K., Van Schmus, W.R. (Eds.), Precambrian: Conterminous U.S. Geol. Soc. Amer., C-2. Boulder, CO, The Geology of North America, pp. 171–334.

Walker, J.D., Klepacki, D.W., Burchfiel, B.C., 1986. Late Precambrian tectonism in the Kingston Range, southern California. Geology 14, 15–18.

Weil, A.B., Van der Voo, R., Mac Niocaill, C., Meert, J.G., 1998. The Proterozoic supercontinent Rodinia: paleomagnetically derived reconstructions for 1100 to 800 Ma. Earth Planet. Sci. Lett. 154, 13–24.

Williams, D.M., Kasting, J.F., Frakes, L.A., 1998. Low-latitude glaciation and rapid changes in the Earth's obliquity explained by obliquity–oblateness feedback. Nature 396, 453–455.

Wright, L.A., Troxel, B.W., Williams, E.G., Roberts, M.T., Diehl, P.E., 1976. Precambrian sedimentary environments of the Death Valley Region, California. In: Troxel, B.W., Wright, L.A. (Eds.), Calif. Div. Mines and Geology, Spec. Rept., 106. Geologic Features of Death Valley, California, pp. 7–15.

Young, G.M., 1995. Are Neoproterozoic glacial deposits preserved on the margins of Laurentia related to the fragmentation of two supercontinents? Geology 23, 153–156.